NANO · MICRO small
www.small-journal.com

The Integration of Magnetic Fields and Catalysts for Clean Energy Conversion

Ziyong Zhang, Bo Feng, Junting Sun, Guowei Li, Zunming Lu, Junqiang Wang,* and Juntao Huo**

Electrocatalysis is a crucial approach for achieving clean energy transitions, requiring highly efficient catalytic materials to expedite this process. However, overcoming the thermodynamic and kinetic constraints is key to discovering next-generation materials that are both cost-effective and efficient. The introduction of magnetic fields offers new opportunities for modulating the electronic structures of catalytic materials, optimizing the adsorption/desorption behavior of key intermediates, and enhancing catalytic efficiency. This review starts with the fundamental principles of classical electrocatalytic reactions, and revisits the main mechanisms by which magnetic fields affect magnetic catalytic materials and electrocatalytic systems, including magneto-thermal effects, magnetohydrodynamic effects, and spin-selective effects. Focusing on amorphous materials, topological materials, and metal oxides, the review highlights the design of magnetic catalytic materials, the control of magnetic structures, and their response behaviors to external fields. Finally, it discusses the major bottlenecks facing magnetic catalysis and its potential applications in other important small molecule catalytic transformations. This review provides a new perspective for understanding the essence of magnetic field chemistry and accelerating the development of catalytic materials aimed at applications.

1. Introduction

With the quick consumption of fossil fuel, the environment and energy crisis triggered the development of clean and sustainable energy sources such as hydrogen, that is advantageous in high energy density and cleanliness. Currently, commercial hydrogen is produced dominantly from fossil fuels, with a relatively small share of green hydrogen.[1] The process of hydrogen production from fossil fuels emits a large amount of carbon dioxide, which requires a high level of hydrogen purification and carbon capture.[2] Green hydrogen, also known as "zero-carbon hydrogen," is hydrogen obtained from electrolysis of water with the electricity coming from renewable energy sources (e.g., solar, wind, nuclear, etc.).[3,4] Water electrolysis involves two key reactions: the hydrogen evolution reaction (HER) at the cathode and the oxygen evolution reaction (OER) at the anode[5] Reducing costs hinges on optimizing the membrane electrode, particularly by lowering the expense of electrode catalysts.[6] While precious metals like Pt, RuO_2, and IrO_x show excellent catalytic performance, their high cost and scarcity limit widespread use.[7]

Generally, the electrocatalytic activity of a catalyst can be tailored from two paths, including increasing the exposed number of active sites and the intrinsic activity of the catalytic active sites.[8] Adjusting the catalyst morphology can improve the active area of the catalyst.[9] The main methods include synthesis of self-supporting structural electrodes through the hydrothermal method, electrodeposition, dealloying, and other strategies, or synthesis of nanoparticles, clusters, tubes, and other catalysts to couple porous matrix materials through sol-gel, high-energy ball milling, laser ablation, etc.[10–20] To increase the intrinsic activity of the catalytic site focuses on adjusting the electronic structure of the catalytic site, through alloying, heteroatom doping, structural modulation (vacancies, strains, heterostructures, etc.) and other engineering of the electronic structure of the active site can effectively affect the adsorption and desorption of the intermediates to enhance the catalytic performance.[21–27] Increasing the number of active sites can enhance reaction rates and material utilization but may lead to uneven activity and reduced stability; improving site activity significantly boosts efficiency and selectivity, though

Z. Zhang, G. Li, J. Wang, J. Huo
Key Laboratory of Magnetic Materials and Devices
Ningbo Institute of Materials Technology and Engineering
Chinese Academy of Sciences
Ningbo 315201, China
E-mail: jqwang@nimte.ac.cn; huojuntao@nimte.ac.cn

Z. Zhang, B. Feng, Z. Lu
School of Materials Science and Engineering
Hebei University of Technology
Tianjin 300130, China
E-mail: luzunming@hebut.edu.cn

J. Sun
Institute of Advanced Magnetic Materials
College of Materials &. Environmental Engineering
Hangzhou Dianzi University
Hangzhou 310018, China

G. Li, J. Wang, J. Huo
Center of Materials Science and Optoelectronics Engineering
University of Chinese Academy of Sciences
Beijing 100049, China

The ORCID identification number(s) for the author(s) of this article can be found under https://doi.org/10.1002/smll.202501973

DOI: 10.1002/smll.202501973

it involves complex preparation and higher costs, and the two are often combined to optimize water electrolysis performance.[28]

The aforementioned engineering approaches primarily focus on the materials themselves, while the introduction of external fields offers new possibilities for enhancing water electrolysis efficiency. Magnetic fields not only affect the charge transport, spin states, and energy levels of catalytic materials but also influence the macroscopic environment of the electrolysis reaction, including solution mass transfer, bubble detachment, and local temperature at the electrodes.[29] As a result, research focus has gradually shifted toward magnetic field-assisted catalysis. In addition to magnetic fields, other external fields also influence the water electrolysis process, including electric fields, strain (stress), light, temperature, and ultrasonic fields.[30–38] Among these, magnetic field-coupled water electrolysis has shown promising research progress in energy efficiency, applicability, and sustainability.[39] This approach provides new opportunities to improve catalytic efficiency and optimize reaction kinetics.

The magnetism of materials mainly comes from the magnetic moment of electrons (spin and orbital motion).[40] When exposed to an external magnetic field, these materials undergo magnetization, and the magnetic moment aligns with the direction of the magnetic field. In paramagnetic materials, the arrangement is weak and temporary, while in ferromagnetic and ferrimagnetic materials, the magnetic domains are redirected, resulting in strong magnetization and hysteresis effects.[41] In addition, magnetic fields can affect the energy state and dynamic behavior of magnetic materials, such as enhancing ion transport in electrolytes or optimizing the adsorption/desorption free energy of reaction intermediates in catalytic processes.[42] These interactions enable the magnetic field to significantly regulate the properties and performance of magnetic materials, thereby affecting the decomposition process of water.

The effect induced by the magnetic field is complex, and there exists the phenomenon of synergistic enhancement of multiple effects.[43] The magnetohydrodynamic effect can accelerate mass transfer, the magnetothermal effect can realize in-situ heating of catalytic sites, and the spin-selective effect can realize selective transfer of electrons.[44] The mutual coupling between magnetic field effects increases the difficulty of studying the mechanism of magnetic-enhanced catalysis. To better understand the promoting effect of magnetic fields on electrochemical reactions, this article introduces the origin and development of material magnetism, as well as the ways in which magnetic fields affect water electrolysis. The possible mechanisms by which magnetic fields affect electrochemical reactions are analyzed, and recent studies on magnetic field-enhanced electrocatalytic reactions are reported. Potential catalyst engineering and materials in the direction of magnetic field-enhanced water electrolysis are summarized. Finally, the future challenges of magnetic field-coupled electrocatalysis are proposed, which is conducive to building excellent electrocatalysts for sustainable energy conversion.

2. Fundamentals of Catalysis and Magnetic Fields

2.1. The Working Principles of Water Splitting Catalysis Reactions

Water splitting consists of two half-reactions: HER at the cathode and OER at the anode. The HER process requires two electrons to complete the reduction reaction, and the source of protons is determined by the pH of the electrolyte. In acidic media, HER proceeds through proton adsorption (Volmer step), followed by electrochemical desorption (Heyrovsky step) or chemical desorption (Tafel step).[45,46] In alkaline media, water molecules are reduced to form hydrogen and hydroxide ions (OH^-). J. K. NØrskov et al. plotted a volcano relationship based on the ΔG_{H^*} of hydrogen by different metals, and Pt was located at the top of the volcano plot, suggesting that Pt has the most moderate adsorption energy for hydrogen.[47] Thus, the second step under the HER mechanism for Pt is usually the Tafel step, and for other metals, it is usually the Heyrovsky step. OER involves the oxidation of water molecules (in acidic conditions) or hydroxide ions (in alkaline conditions) to generate oxygen gas (O_2). OER is characterized by multiple intermediate steps, including the formation of adsorbed hydroxyl (OH*) and oxo (O*) species, which combine to form O_2.[7, 48–50] Due to its high overpotential and slow kinetics, OER is often the rate-limiting step in water splitting.[51] Existing studies have suggested that the adsorption/desorption strength of oxygen-containing intermediates is the key factor affecting the OER mechanism.[52] The catalytic mechanism of OER can be classified into the adsorbed oxygen evolution mechanism (AEM), the lattice oxygen-mediated mechanism (LOM), and the oxygen-oxygen coupling mechanism (OPM), based on the differences in the active sites of the adsorbed intermediates.[52–55]

2.2. Brief Overview of Magnetic-Related Phenomena

Human understanding of magnetic fields and materials dates back to around 400 BC with the invention of the sinan, an early compass (**Figure 1**). The 18th and 19th centuries saw significant progress in electricity and magnetism, highlighted by Michael Faraday's discovery of electromagnetic induction in 1831, which linked electricity and magnetism and laid the foundation for their intersection with electrochemistry.[56] In 1847, William Thomson (Lord Kelvin) introduced the "Kelvin force," a concept central to magnetohydrodynamics (MHD), derived from his studies on electromagnetism and fluid mechanics.[57] Subsequent discoveries, such as the magnetoresistance effect (1856),[58] the Maxwell stress tensor, the magnetocaloric effect (1881),[59] and the Lorentz force equation (1892), further advanced the field.

In the 20th century, people's understanding of magnetic phenomena became more profound. In 1921, Arthur Compton proposed that electrons might possess a "spin" property to explain magnetic phenomena, advancing the development of quantum mechanics and influencing materials science, information technology, and energy research.[60] In 1942, Hannes Alfvén introduced the concept of magnetohydrodynamic waves, demonstrating that magnetic fields could influence the motion of conductive fluids and deriving the fundamental equations of MHD.[61] In the 1960s, T. Z. Fahidy conducted systematic research on the effects of magnetic fields on fluid flow and mass transfer in electrolytes, providing critical insights into the coupling of magnetic fields with water electrolysis reactions. Over the following decades, researchers recognized that magnetic fields influence water electrolysis through multiple complex mechanisms, leading to diverse studies in this field. These efforts have significantly advanced the understanding of magnetic field-enhanced

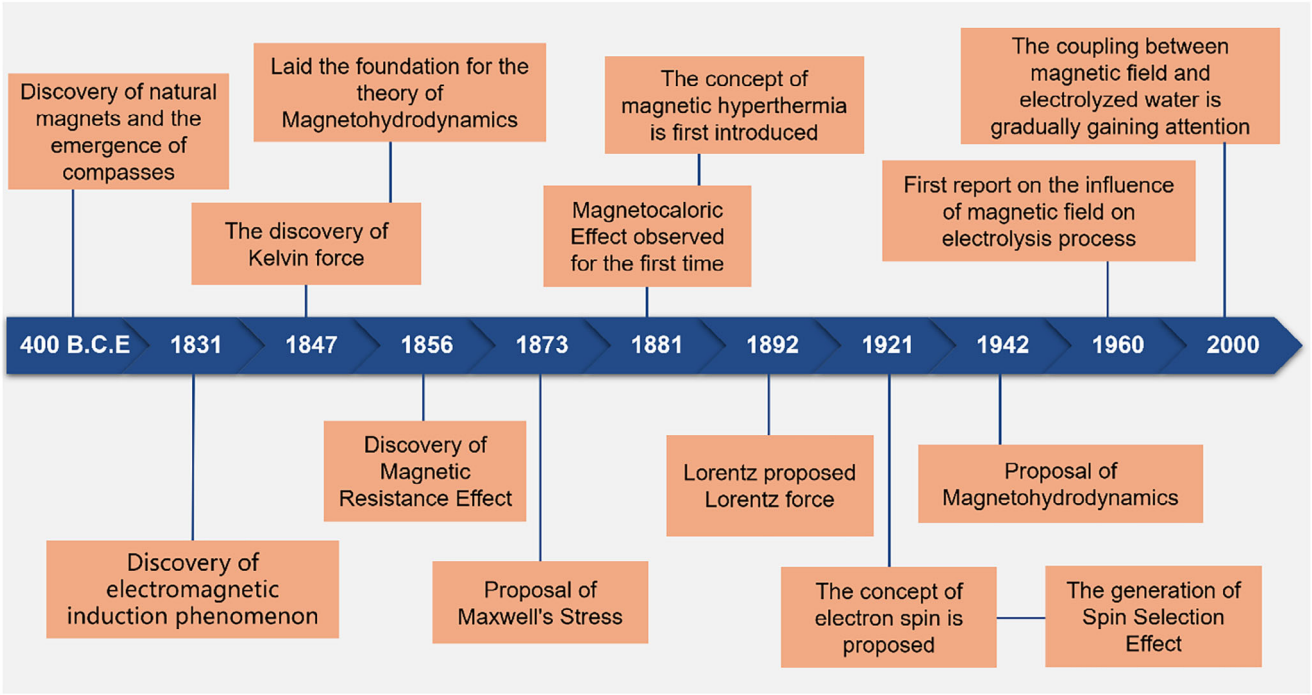

Figure 1. The development history of magnetic-related phenomena.

electrochemical processes. It also provides a lot of theoretical support for our further exploration in this field.

2.3. Types of Magnetic Fields During Catalysis

The application of magnetic fields in water electrolysis can be categorized and optimized based on their types and parameters to achieve efficient regulation of the reaction process.[62] Magnetic fields are mainly classified into static magnetic fields, alternating magnetic fields, pulsed magnetic fields, and gradient magnetic fields.[63] Static magnetic fields, generated by permanent magnets or DC electromagnets, are suitable for studying the steady-state effects of magnetic fields on water electrolysis, such as enhancing ion transport and optimizing electrode surface reaction kinetics. Alternating magnetic fields, produced by AC electromagnets, vary in strength and direction over time, making them ideal for dynamic regulation, such as inducing eddy currents in the electrolyte and promoting bubble detachment from the electrode surface. Pulsed magnetic fields, characterized by high intensity and short duration, are effective for rapidly altering ion distribution and increasing reaction rates. Gradient magnetic fields, which exhibit spatial variations in strength, are suitable for locally optimizing ion transport paths and enhancing reaction activity.

Key parameters of magnetic fields include strength (typically ranging from 0.01 T to over 1 T), direction (parallel, perpendicular, or at an angle to the electrode surface), frequency (from 1 Hz to over 10 kHz), and duration (from seconds to days). Magnetic field strength directly influences the magnitude of Lorentz forces and magnetohydrodynamic effects, while the direction determines the flow patterns of the electrolyte and bubble behavior. Frequency and duration affect the dynamic effects of alternating magnetic fields and the cumulative effects of magnetic fields, respectively. Through experimental design and theoretical modeling, these parameters can be optimized to maximize the regulatory effects of magnetic fields on water electrolysis. For example, moderate-strength parallel magnetic fields can significantly enhance mass transfer efficiency, while high-frequency alternating magnetic fields effectively reduce bubble-induced overpotential. By rationally selecting and optimizing the type and parameters of magnetic fields, the efficiency and performance of water electrolysis can be significantly improved, providing new research directions for developing efficient and low-energy hydrogen production technologies.

In summary, the coupling between magnetic fields and water splitting provides a promising strategy to enhance the efficiency of HER and OER. By elucidating the underlying mechanisms and optimizing magnetic field application methods, researchers can advance sustainable hydrogen production technologies.

2.4. Magnetic Fields and Key Reaction Intermediates

The reaction intermediates play a crucial role in understanding and designing efficient catalysts for water splitting.[64] From the basic reaction steps of HER, electron transfer and hydrogen adsorption (H*) play a key role.[47] In this case, hydrogen atoms need to undergo complex adsorption and desorption processes on the catalyst surface, so the binding energy between hydrogen atoms and the active site should be neither too weak nor too strong.[65] In OER, intermediates such as OH*, O*, and adsorbed peroxide (OOH*) determine the reaction pathway and overpotential.[66] Due to the linear relationship of the binding

energy of the intermediates, the difference between ΔG_{*OH} and ΔG_{*O} of the catalyst was utilized to establish a volcano plot between $\Delta G_{O*} - \Delta G_{OH*}$ and overpotential η.[67] In addition to this, some other activity descriptors, such as metal site d-band enters, e_g electron filling number, etc. have a typical volcano relationship with the OER overpotential.[68,69] These studies suggest that the moderate bonding strength of the catalytically active centers to the intermediates facilitates the adsorption and desorption of the reaction.

Catalytic reactions are closely related to the electronic configuration of the active site and reaction intermediates. In the field of oxygen electrocatalysis, the ground state of the oxygen molecule is a triplet state, with the front Π* orbitals occupied by two parallel-aligned electrons, in contrast to the spin state of OH^-/H_2O, which is a singlet state. From OH^-/H_2O to O_2 (OER), the participation of O_2 requires spin-dependent electron transfer.[70] Due to the significant difference in the thermodynamic states of singlet and triplet oxygen, the lowest excited state of O_2 is a singlet, and the ground state is a triplet, with the ground state being more than 1 eV lower in energy than the excited state.[71] The OER reaction intermediate oxygen exists in a singlet state, and quantum mechanics suggests that electrons do not jump between two different spin states. So the high overpotential of OER can be attributed to this; the paramagnetic state of O_2 needs to be generated in the antimagnetic excited state and slowly decay to the ground state through a higher energy process, and the catalytic reaction in the spin-conserving magnetic ground state will greatly improve the catalytic efficiency.[72]

Magnetic fields significantly influence the behavior of reaction intermediates, such as H* and oxygen-containing intermediates, during water splitting. By modulating the spin states of electrons, magnetic fields can alter the adsorption and desorption kinetics of these intermediates on the catalyst surface. This spin selectivity effect optimizes the reaction pathways, reducing the energy barriers for intermediate formation and conversion. For HER, the magnetic field can regulate the electronic structure of the catalyst surface, making the adsorption energy of H* closer to the thermal neutral value. Spin polarization can accelerate the coupling process of H * intermediates and reduce the energy barrier for H_2 molecule formation.[73] For OER, magnetic fields can enhance the transition from OH* to O* intermediates, thereby accelerating the overall reaforon rate. Current research indicates that the magnetic field affects the spin-polarization kinetics of water splitting starting from the first step of electron transfer, and the ferromagnetic exchange between the ferromagnetic catalyst and the adsorbed oxygen species occurs under the principle of the conservation of spin angular momentum.[74] The influence of the magnetic field on the OER tachyon step is confirmed by analyzing the change of the Tafel slope under the magnetic field. The stronger 3d-2p hybridization between the catalyst and the adsorbed oxygen species after spin polarization is more conducive to the transfer of spin-polarized electrons (**Figure 2**a–c).

2.5. Ions Transport and Bubbles Release

The presence of a magnetic field exerts Lorentz forces on charged species, such as H^+ and OH^- ions, in the electrolyte. These forces alter the trajectories of ions, enhancing their mobility and promoting more efficient mass transport. This effect reduces concentration polarization near the electrode surface, ensuring a steady supply of reactants and removal of products. In HER, for example, the improved transport of H^+ ions to the cathode surface under a magnetic field can significantly enhance the reaction rate. Similarly, in OER, the increased mobility of OH^- ions facilitates their oxidation at the anode, contributing to higher overall efficiency. Magnetic fields also impact the behavior of gas molecules, such as H_2 and O_2, generated during water splitting. By inducing micro-convection in the electrolyte, magnetic fields promote the detachment of gas bubbles from the electrode surface. This minimizes bubble accumulation, which can block active sites and increase overpotential. For instance, in HER, the rapid removal of H_2 bubbles from the cathode surface ensures continuous exposure of active sites, enhancing reaction efficiency. Similarly, in OER, the detachment of O_2 bubbles from the anode surface reduces bubble-induced resistance, improving the overall performance of the electrolysis process. Furthermore, magnetic fields can influence the nucleation and growth of gas bubbles, optimizing their size and distribution for more efficient release.

We conducted a systematic study on the influence of an alternating magnetic field (AMF) on HER using $Fe_{29}Co_{29}Ni_{29}P_{3.9}B_{9.1}$ alloy ribbons as the research subject. The AMF significantly enhanced the catalytic efficiency of the HER, with a 27% increase in current density at 20 mT. This improvement is attributed to the Lorentz interaction enhancing charge transfer efficiency, while the contribution of the heating effect is minimal. The high magnetic permeability of the Fe–Co–Ni—P–B electrode and the skin effect of electromagnetic eddy currents can amplify the Lorentz effect (Figure 2d,e).[75] In addition, studies have shown that the coverage of fractional bubbles is strongly delayed in the presence of an external magnetic field. Therefore, due to the availability of more active sites for the reduction process, the current density has increased. These effects are discussed regarding the Lorentz force-driven convection caused by magnetic fields (Figure 2f,h).[76] To further address the influence of magnetic fields applied in vertical electrode configurations, where the bulk Lorentz force can be ignored, numerical studies have been conducted. This reveals the improved mechanism of hydrogen bubble desorption from the electrode surface.

3. The Physical Basis for Magnetic Fields Tailored Electrochemical Reactions

The main existing magnetic enhanced catalytic performance effects that have been studied mainly include the magnetohydrodynamic effect, the magnetothermal effect, and the spin-selection effect, while other magnetic enhancement effects such as the magnetoresistance effect, the Maxwell stress effect, the Kelvin force effect, and the Gibbs-free energy effect have been less studied. In this section, we briefly summarize the mechanism of these magnetic effects on catalysis.

3.1. Magnetothermal Effect

The magnetothermal (MT) effect is the localized heating phenomenon that occurs when an alternating magnetic field acts on

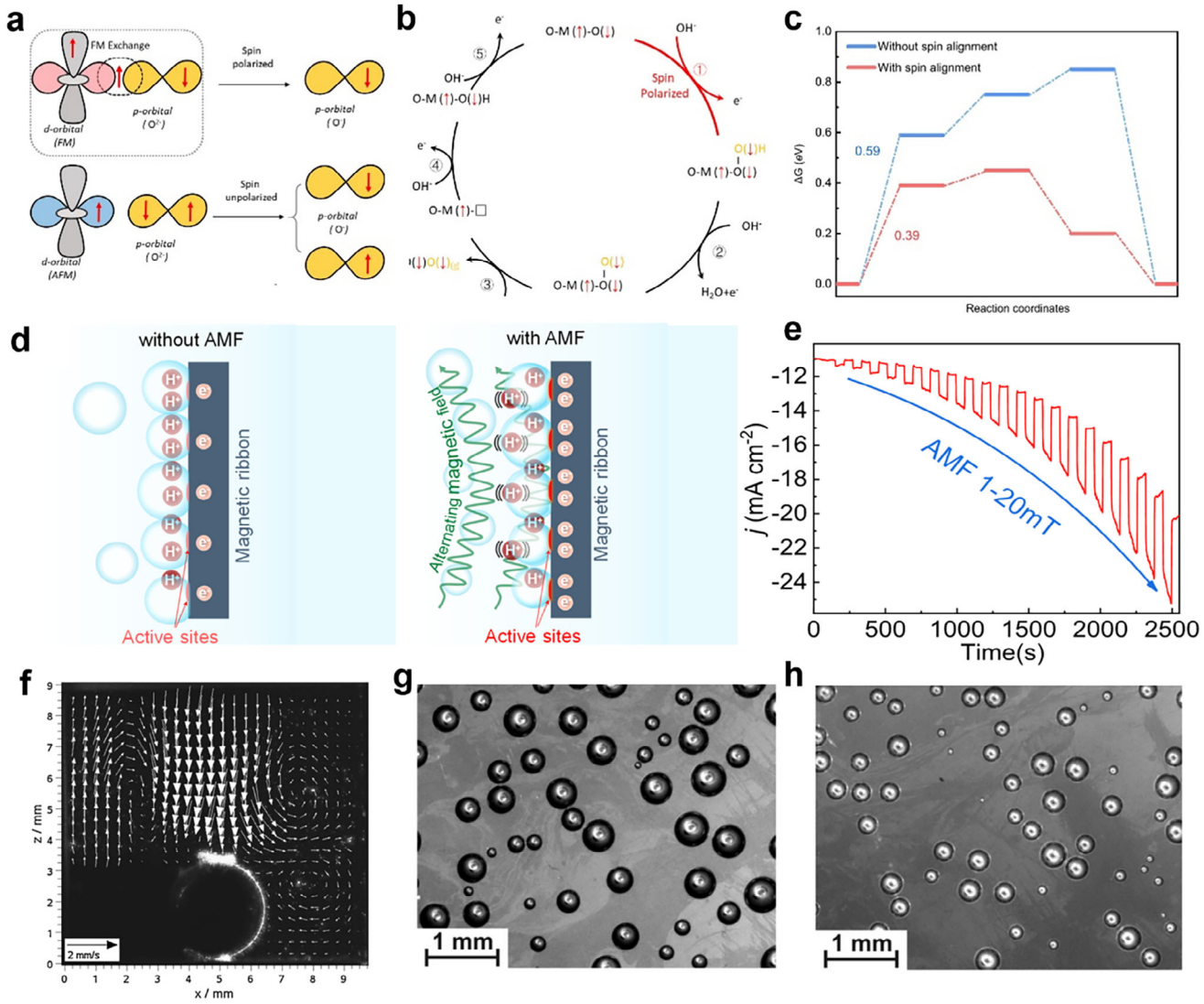

Figure 2. a) Ferromagnetic exchange interaction of $CoFe_2O_4$ promotes spin-polarized electron transfer; b) OER path of spin-polarized electron transfer; c) OER Gibbs free energy change before and after spin-polarization; Adapted with permission.[74] Copyright 2021, Springer Nature. d) Schematic illustration of the critical role of the AMF in increasing the HER activity. e) At a fixed overpotential, the changes in current density (Δ_j) with or without sAMF of various intensities (H_0) from 1 to 20 mT; Adapted with permission.[75] Copyright 2022, American Chemical Society. f)Velocity distribution around an artificial bubble under the superposition of a vertical homogeneous magnetic field. Hydrogen bubbles formed at the electrode surface in the stationary regime observed without a magnetic field (g) and in the perpendicular to the electrode magnetic field (h). Adapted with permission.[76] Copyright 2011, Elsevier.

magnetic nanoparticles, and it works by using an external high-frequency alternating magnetic field to achieve localized heating on magnetic nanoparticles.[77] According to the Arrhenius equation:

$$k = Ae^{-E_\alpha/RT} \quad (1)$$

where k is the reaction rate constant, A is the frequency factor; E_α is called the experimental activation energy; R is the molar gas constant, and T is the thermodynamic temperature.

The reaction rates of electrochemical reactions are significantly affected by their kinetic barriers and mass transfer efficiencies, and since these reactions are extremely sensitive to temperature changes, the operating temperature becomes a key factor in regulating the HER and OER rates. The enhancement of the catalytic reaction rate by the magneto-thermal effect can be attributed to the synergistic effect of lowering the resistance to charge transfer, facilitating bubble removal, and increasing the charge energy state.[78] By applying a high-frequency alternating magnetic field to FeC–Ni NPs to achieve in-situ heating of the catalyst (**Figure 3**).[79] The results show that the magnitude of the enhancement of the reaction kinetics is equivalent to heating the overall electrolytic cell temperature to 200 °C, but the electrolytic cell temperature only increases by 5 °C. The local temperature of magnetothermal nanoparticles is much higher than that predicted by the diffusion equation, and the

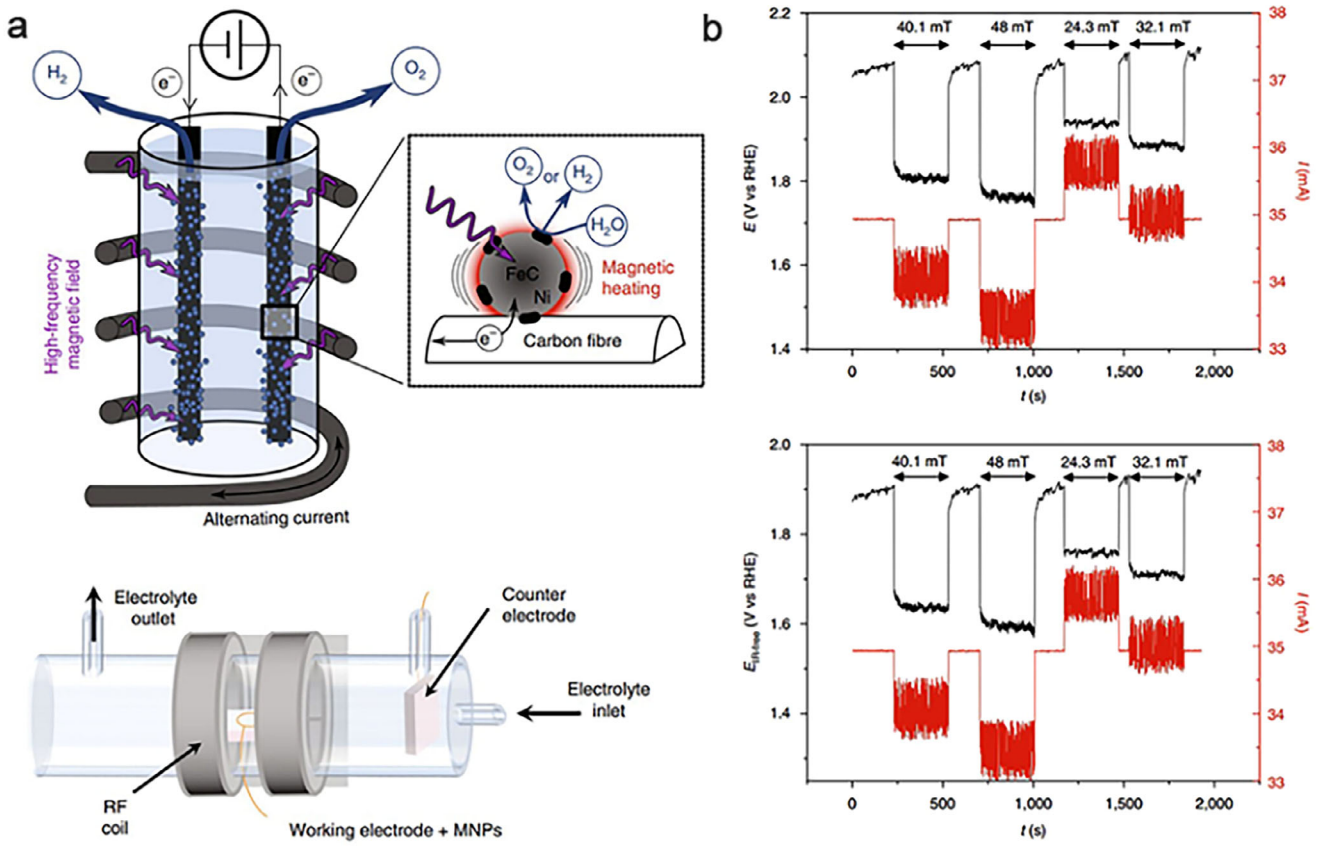

Figure 3. a) Principle of localized heating enhancement of electrolytic water by the magneto-thermal effect of metal nanoparticles under alternating magnetic field. b) Effect of alternating magnetic field on potential and current of FeC-Ni OER electrode. Adapted with permission.[79] Copyright 2018, Springer Nature.

energy consumed to heat the catalyst in situ is much lower than that required to heat the entire energy conversion device to the same temperature, with relatively less damage to the electrode material.

There are two mechanisms of magnetic heating of ferromagnetic nanoparticles: Brownian relaxation and Neel relaxation. Brownian relaxation is the structure of the physical rotation of ferromagnetic nanoparticles, where the internal magnetic moment tends to coincide with the external magnetic field; Neel relaxation is the result of flipping the magnetic moment along the direction of the external magnetic field.[80] Huang et al. introduced Se vacancies into $NiSe_2$ nanoparticles with ultra-small particle sizes, and the introduction of Se vacancies lowered the reaction energy barriers and also induced ferromagnetism in $NiSe_2$ nanoparticles, and showed that catalyst nanoparticles produced Neel relaxation-related localized magnetic heating due to spin flips of the magnetic domains, and the HER overpotential was reduced by 40 mV at 10 mA cm^{-2}, and the current density was increased by 400% at a 180 mV potential increased the current density by 400% (**Figure 4a**).[81] Yuan et al. developed a two-step synthesis process to fabricate NiFe/NiFeOOH core-shell nanoparticles. Initially, NiFe nanoparticles were deposited on a carbon substrate using pulsed laser deposition. Subsequently, these nanoparticles were electrochemically reconfigured to form NiFe/NiFeOOH core-shell structures. By employing Néel relaxation-related magnetic heating under an alternating magnetic field, the researchers achieved a significantly reduced oxygen evolution reaction (OER) overpotential of 209 mV. This innovative approach resulted in a remarkable 133 mV decrease in OER overpotential at a current density of 10 mA cm^{-2} (Figure 4b).[82]

In situ heating of the catalyst using a magnetic field can avoid damage to the electrode material. Liu et al. coordinated organic ligands and magnetic transition metals to form an organometallic framework material and used organic molecules with low thermal conductivity to construct an insulating layer, thereby confining magnetic heating to the metal active center (**Figure 5a–c**).[83] Under the magnetothermal effect, the crystal field splitting energy increases, and the energy difference between the e_g and t_{2g} orbitals becomes larger, inhibiting the interorbital electron leaps to transform the metal into a low-spin state. Using the magnetic exchange effect to drive the spin-flip and reconfiguration of the metal ions, the OER overpotential decreased by 120 mV at 100 mA cm^{-2} current density after the high-frequency alternating magnetic field was applied for 20 min. Compared with thermal annealing of the catalysts, this design excludes the thermal strain perturbation generated by the transformation of the magnetic structure and enables long-time stability to be achieved. The introduction of Ni nanoparticles into amorphous iron hydroxide nanosheets can act as magnetic heating centers under the AC

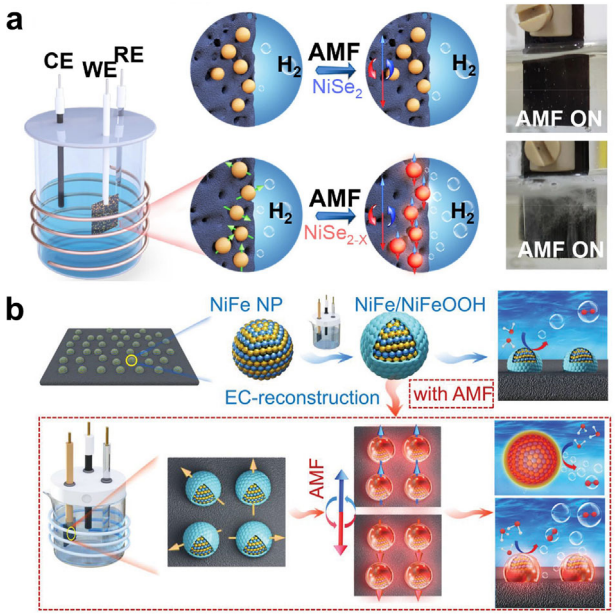

Figure 4. a) Schematic and real pictures of $NiSe_2$ NPs and $NiSe_{2-X}$ NPs with AMF stimulation; Adapted with permission.[81] Copyright 2023, Elsevier. b) Schematic diagram of the EC-reconstruction and AMF-based magnetic heating effect. Adapted with permission.[82] Copyright 2022, John Wiley and Sons.

magnetic field. The localized heating around the Ni nanoparticles could improve the rate of the reaction and further facilitate the adsorption of the reaction intermediates, which can achieve efficient energy transfer and good durability (Figure 5d).[84] The overpotential of a-NiFe@Ni-CW at 100 mA cm^{-2} under an AC magnetic field is 268 mV, which is superior to most reported transition metal catalysts.

3.2. Magnetohydrodynamic Effect

The gas precipitation reaction will inevitably produce a large number of bubbles, due to the net magnetic force, the resulting bubbles attached to the electrode surface, the active area of the electrode will be reduced, affecting the specific area of the activity of the magnetohydrodynamic effect is caused by the Lorentz force in the ionic aqueous solution or electrolyte on the macroscopic or microscopic convection. According to the left-hand law, the Lorentz force (F_{Lore}) can be expressed as:

$$F_{Lore} = j \times B \quad (2)$$

where j is the current density and B is the magnetic field. Thus, the direction of the Lorentz force can be controlled by changing the angle between the magnetic field and the electric field, and the magnitude of the Lorentz force can be enhanced by increasing the strength of the magnetic field (B) and the applied potential (E).

The moving charged particles will be subjected to the Lorentz force under the magnetic field, which generates convection under the interaction of the magnetic field and the local current, accelerating the transport of electroactive substances to the electrode surface.[85] When the magnetic field is parallel to the electrode surface and the Lorentz force is in the same direction as the buoyancy force, it is favorable for bubble separation.[86] Rapid separation of bubbles in the interfacial region refreshes the active region in time as well as improves the conductivity of the electrolyte-catalyst interface by reducing the porosity. The type of magnetic field will directly affect the effect of magnetohydrodynamic effect, if it is a constant magnetic field adjusting the size and angle of the magnetic field can get a stable magnetic enhancement, if it is an AC magnetic field, the direction and size of the magnetic field is constantly changing, the convective flow velocity gradient is more complex, the enhancement of the magnetohydrodynamic effect is unstable (**Figure 6**a,b).[44] Xiao et al. directly observed bubble acceleration perturbations due to AC magnetic field-induced magnetohydrodynamic convection at the electrode surface, and concluded that magnetohydrodynamic convection reduces the thickness of the diffusion boundary layer and accelerates mass transfer, and that, as the intensity of the AC magnetic field is increased, it generates larger eddy currents between the electrodes and inhibits the transport of electroactive material to the electrode surface (Figure 6c).[87]

The alloys usually exhibit strong ferromagnetism and are more sensitive to magnetic field response. Compared with pure metal catalysts, metal alloys have better electrocatalytic HER activity due to strain effects and synergistic effects on the modulation of crystal structure and electronic structure. Metals such as Fe, Co, and Ni can be alloyed to enhance the intrinsic activity of the active sites, and the synergistic effect between the metals can optimize the metal-hydrogen binding energy.[89] Hedge et al. reported the HER properties of NiW alloys due to the magnetohydrodynamic effect induced by the Lorentz force, eliminating the bubbles on the electrode surface and reducing the overpotential.[90] Magnetohydrodynamic effects are prevalent in magnetically enhanced OER processes. Peng et al. synthesized Co_3O_4 on nickel foam (NF) by hydrothermal as well as subsequent thermal treatments. The overpotential at 20 mA cm^{-1} was reduced from 308 to 252 mV under a magnetic field of 125 mT, and the overpotential decreases with the increase of the magnetic field. The decrease in the slope of the Tafel indicates that the OER charge transfer coefficient is higher and has a lower activation energy. The magnetic field can induce the MHD effect near the electrode and promote charge transfer in the catalytic process, and the effect is greatest when the direction of the electric and magnetic fields are perpendicular to each other (Figure 6d,e).[88] Fan et al. found that the OER overpotential of NiFe-layered double hydroxide (LDHs) was reduced by 42 mV at a magnetic field of 200 mT, attributed to the magnetic field-induced magnetohydrodynamic effect and electrode/electrolyte charge transfer.[91]

Oxygen vacancy-modified $ZnCo_2O_4$ led to the generation of partially divalent cobalt ions and ferromagnetism because of the ferromagnetic exchange between Co^{2+}-O-Co^{3+} of the catalysts.[92] The overpotential of 10 mA cm^{-2} was reduced by 117 mV under an alternating magnetic field of 4.75 mT. Due to the concentration gradient distribution of oxygen vacancies in the bulk phase of the catalyst, a built-in electric field will be formed inside the catalyst, and the susceptibility potential generated by

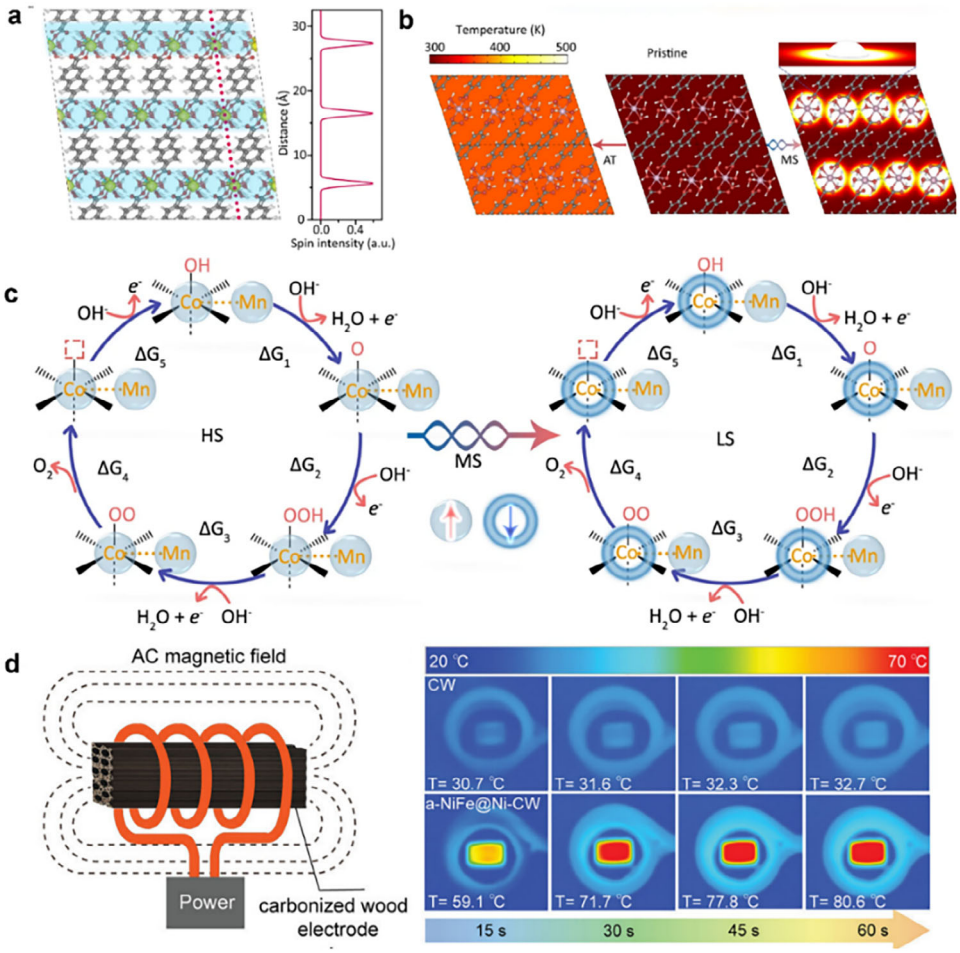

Figure 5. a) Spin density distribution of $Co_{0.8}Mn_{0.2}$-MOF; b) Theoretical simulation of the conventional annealing treatment versus magneto-thermal process; and c) The mechanism of OER of Co sites with different spin configurations. Adapted with permission.[83] Copyright 2021, Springer Nature. d) Schematic of a-NiFe@Ni-CW for OER under the AC magnetic field and infrared photographs of CW and a-NiFe@Ni-CW, corresponding to t = 15, 30, 45, and 60 s in order from left to right. Adapted with permission.[84] Copyright 2023, John Wiley and Sons.

the applied magnetic field on the surface of the catalyst is superimposed on the built-in field to obtain a higher-intensity electric field gradient, which is capable of lowering the reaction energy barriers and enhancing the charge transfer rate (**Figure** 7a).

Gao et al. synthesized catalysts with a non-homogeneous $NiFe_2O_4$@(Ni, Fe)S/P core-shell structure using spinel $NiFe_2O_4$ microspheres as the substrate and sulfide/phosphorization treatments, and the overpotential was reduced by 45.5% under an alternating magnetic field (Figure 7b).[93] The Faraday induction potential generated by the alternating magnetic field induces the enrichment of active ions OH^- on the electrode surface; under low current, the catalytic reaction is importantly controlled by the charge transfer process, and the enrichment of OH^- on the electrode surface undoubtedly accelerates the charge transfer efficiency; under high current, the catalytic reaction is mainly affected by the diffusion process, and the enrichment of OH^- attenuates the diffusion of ions in the electrolyte solution, and the low diffusion rate leads to the decrease in the catalytic performance.

Bidin et al. investigated the Lorentz force on water molecules, where electrons form eddy currents in the presence of an applied magnetic field, which generates an induced magnetic field in the opposite direction of the applied magnetic field, B_I. This opposing magnetic field generates a repulsive force, which leads to the stretching of water molecules under the repulsive force, and consequently, to the rupture of hydrogen and covalent bonds (Figure 7c–g). this repulsive force mechanism can be effectively applied when the strength of the external magnetic field reaches 47 mT. Promotes the electrolysis of water molecules and significantly reduces the reaction energy barrier, which improves the oxygen precipitation efficiency by about six times.[94]

3.3. Kelvin Force Effect

Unlike the Lorentz force, which affects convection at different length scales, the Kelvin force (F_K) may have a significant effect on ferromagnetic microelectrodes and nanostructured

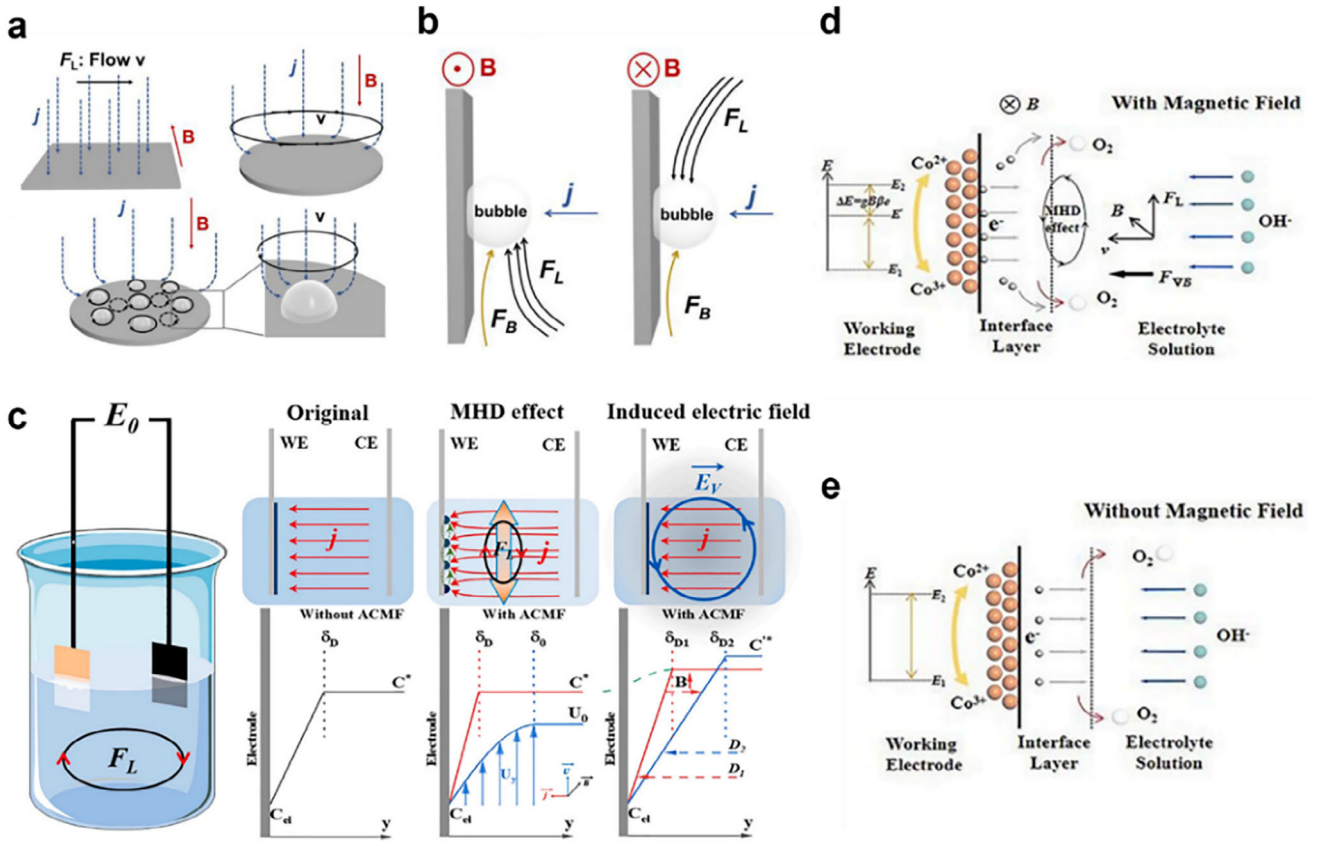

Figure 6. Magnetohydrodynamic effects in a uniform magnetic field. a) Different magnetohydrodynamic perturbations are produced by a magnetic field perpendicular or parallel to the current. b) Micro-magneto-fluid is generated around a bubble. Adapted with permission.[44] Copyright 2020, American Chemical Society. c) Magnetohydrodynamic effects induced by an alternating magnetic field on the diffusion layer. Adapted with permission.[87] Copyright 2021, Elsevier. d,e) Mechanisms of magnetic field enhancement of Co_3O_4/NF OER performance. Adapted with permission.[88] Copyright 2019, Elsevier.

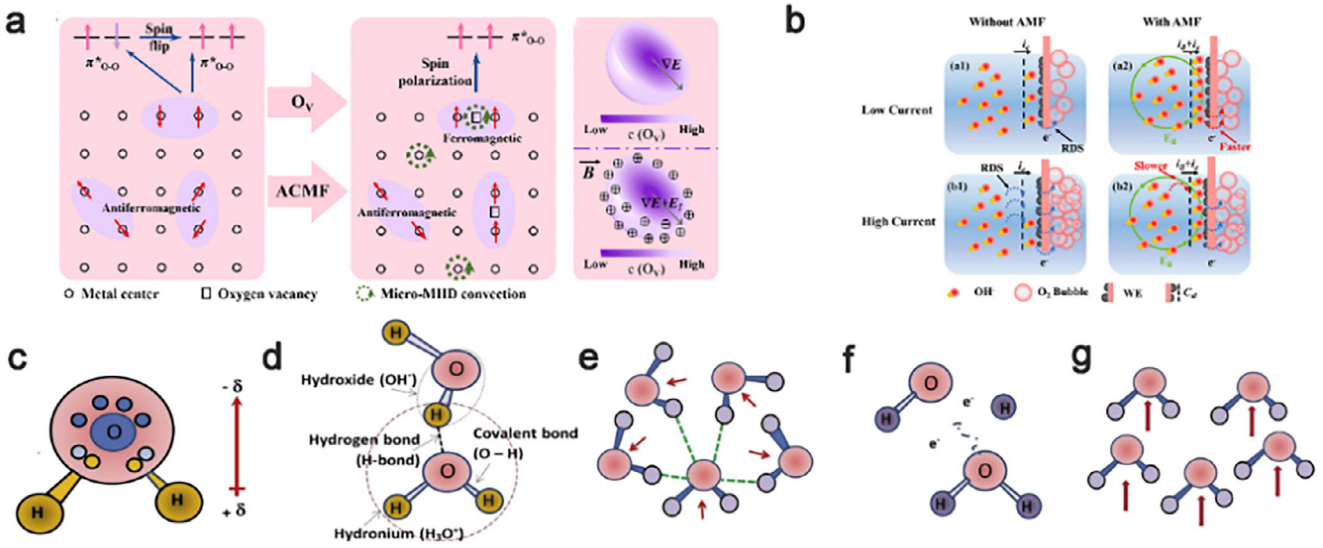

Figure 7. a) Schematic illustration of the mechanism of the improvement of the performance of OERs by oxygen vacancies under an alternating magnetic field. Adapted with permission.[92] Copyright 2024, Elsevier. b) Schematic representation of the effect of the mechanism. Adapted with permission.[93] Copyright 2023, American Chemical Society. c) Molecular structure of water. d) Autoprotolysis phenomenon; formation of hydronium and hydroxide ions in the absence of an electric field. e) Networking of hydrogen bonding (green dash line) in water molecular structure, which creates unpolarize dipole moment (red arrows) (f) water ionization; dissociation of water molecule into in proton and hydroxide and the release of electrons (g) The polarization of dipole moment (upright arrows) after reaction with an electric field. Adapted with permission.[94] Copyright 2017, Elsevier.

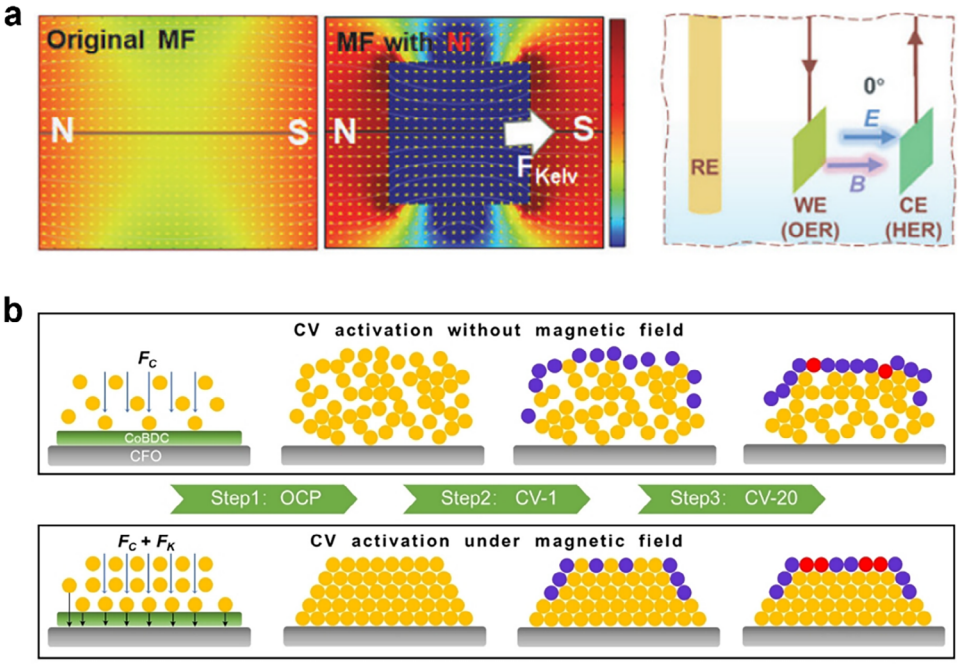

Figure 8. a) Simulation of the magnetic field in air and its redistribution due to the presence of the electrode plate. Adapted with permission.[97] Copyright 2023, Elsevier. b) Schematic modeling of the conformational evolution of Co sites under CV activation. The yellow, blue, and red spheres represent Co^{2+}, Co^{3+}, and Co sites with oxygen vacancies, respectively. Adapted with permission.[99] Copyright 2024, John Wiley and Sons.

ferromagnetic arrays, usually acting on magnetic materials or objects with magnetic moments. The Kelvin force is a force induced by a gradient magnetic field that leads to convection on a surface with a gradient magnetic field, which can be expressed as:[95]

$$F_K = \frac{1}{2\mu_0} c\chi_m \nabla B^2 \tag{3}$$

where μ_0 is the free space permeability; ∇B is the magnetic field gradient; χ_m is the molar magnetization rate, and c is the volumetric concentration of the electrochemically active substance.

In redox processes, the transfer of electrons usually involves paramagnetic substances such as free radicals, paramagnetic cations, and molecules with unpaired spins, which can be propelled by the Kelvin force to regions of higher magnetic density. Farmani et al. designed a bulk Ni thin-film catalyst with a mesoporous structure, which can achieve OER performance close to that of a noble-metal electrode at an applied magnetic field. Their computational simulations show that the porous structure enhances the magnetic field gradient on a microscopic scale, which can be obtained on a 10^{-7} T m^{-1} scale with an external magnetic field of 0.2 T. This high steepness of the gradient magnetic field effectively promotes the attraction/repulsion of paramagnetic ions and bubbles as well as the decomposition of antiferromagnetic water molecules.[96] Li et al. deposited superhydrophilic γ-Fe_2O_3 layers on different electrode substrates and analyzed the effect of the magnetic field on oxygen bubble release. They found through finite element simulations that when the electrodes were inserted in a uniform magnetic field, the magnetic field redistribution was severe, relatively weak in the electrode plate itself and the upper and lower spaces, but strong in the left and right spaces, which generated a gradient magnetic field around the surface reaction zone, and the Kelvin force formed forced the paramagnetic O_2 to move, thus promoting the release of O_2 (**Figure 8**a).[97] In metal-air batteries and fuel cells, the cathodic reaction usually uses air as the feedstock, while other components in air and products of liquid water may occupy the active center, hindering the reduction of O_2 on the catalyst surface and leading to concentration polarization. The attraction of the Kelvin force to paramagnetic oxygen realizes oxygen enrichment on the electrode surface, which avoids the blockage of antimagnetic N_2 or H_2O on the electrode surface and provides more channels for oxygen transport to improve the reaction efficiency.[98]

Due to the directional movement of paramagnetic material under a gradient magnetic field, the thickness of the diffusion layer changes locally during the electrodeposition of metals, making the distribution pattern of the deposits show consistency with the magnetic field distribution. In regions of higher magnetic field strength, ions with larger magnetization tend to concentrate more, leading to an increase in the thickness of the deposited layer, while in regions of weaker magnetic fields, the deposits may be thinner. The Kelvin force can also significantly affect the convective behavior in the diffusion layer during electrodeposition. While the stability of the diffusion layer is usually regulated by a combination of diffusion, convection, and deposition reaction rates, the Kelvin force can further modulate the local convection pattern by interacting with natural convection and Lorentz forces in solution. This effect is particularly significant under non-uniform magnetic field conditions, and experiments with hexagonal magnet arrays by Dunne et al. have shown that the magnetic field gradient can significantly enhance the

concentration of the deposit in a specific region, leading to the controllability of the deposit morphology.[96] In addition, the phenomenon of surface remodeling of electrochemically active substances inevitably occurs during electrochemical reactions, and the use of gradient magnetic fields for directional manipulation of paramagnetic substances generated in the process of surface remodeling can selectively regulate the active substances. Ma et al. designed a ferromagnetic/nonmagnetic $CoFe_2O_4$@CoBDC core-shell catalyst, where an applied magnetic field could generate a localized gradient magnetic field in the ferromagnetic $CoFe_2O_4$, and the induced Kelvin force directionally regulated the CoBDC surface remodeling, leading to the directed aggregation and relatively regular stacking of paramagnetic Co^{2+} on the surface of the $CoFe_2O_4$, followed by a first CV cycle whereby some Co^{2+} ions were irreversibly oxidized to Co^{3+}. Finally, Co^{2+} and Co^{3+} undergo a series of redox reactions, and the additional energy of the magnetic field thermodynamically stabilizes the high-spin state Co^{2+} and prevents the transition from Co^{2+} to Co^{3+}, leading to a higher proportion of highly reactive Co^{2+} in the derived CoOxHy (Figure 8b). The reconfigured catalysts exhibit significantly enhanced OER performance, with overpotentials at a current density of 10 mA cm^{-2} decreased by 28 mV.[99]

3.4. Maxwell Stress Effect

Maxwell stress (Maxwell stress) is the stress that occurs in an electromagnetic field due to the interaction of the electric and magnetic fields. This stress can exert a force on the fluid medium in a water electrolysis system, which in turn changes the flow characteristics of the fluid and the reaction environment at the electrode surface.[100] In a reaction system for the electrolysis of water, when a magnetic field is applied, the charged particles in the liquid and the reacting material are subjected to an electromagnetic force in the magnetic field. Maxwell's stress is used to describe the distribution of this force with the equation:

$$T_{ik} = \varepsilon_0 \left(E_i E_k - \delta_{ik} \frac{E^2}{2} \right) + \frac{1}{\mu_0} \left(B_i B_k - \delta_{ik} \frac{B^2}{2} \right) \quad (4)$$

where E and B are the vectors of the electric and magnetic fields, respectively, ε_0 and μ_0 are the dielectric constant and magnetic constant, respectively, and δ_{ik} is the Kronecker δ function.

Maxwell stress affects the stability and ion mass transfer efficiency of the double electronic layer by altering the electric field distribution and also modulates the motion and distribution of electrons on the electrode surface, which ultimately improves the rate and efficiency of electrochemical reactions. When an applied magnetic field is applied to an electrolyte solution, the stress due to the magnetic field changes the potential gradient in the vicinity of the electrode, which leads to a readjustment of the charge distribution within the bilayer.[101] Changes in the electric field distribution can affect the speed and direction of ion movement, thus regulating the thickness and structure of the bilayer.[102] The electrochemical double-layer capacitance is an important parameter for the evaluation of electrocatalytic reactions, and changes in the electrochemical double-layer capacitance lead to different electrochemically active surface areas, which affect the electrochemical reaction.[103]

Paramagnetic droplets can be stretched transversely or longitudinally under a magnetic field, and Maxwell stresses can act on paramagnetic radicals in solution close to the electrodes, leading to positional migration of the outer Helmholtz surface and thus affecting the electrochemical double layer.[104] The hydrodynamic changes induced by Maxwell stress can also accelerate the local flow of the electrolyte solution and promote the exchange of ions in the bilayer region. This acceleration reduces the retention time of ions on the electrode surface and improves the transfer efficiency of ions to the active sites of the electrode, which in turn increases the electrochemical reaction rate.[105] On the other hand, the electromagnetic force induced by Maxwell stress on the electrode surface can affect the movement path of electrons and induce the redistribution of electrons on the electrode surface. This effect can effectively reduce the electron accumulation region and optimize the electron supply to the active region of the electrode.

3.5. Magnetoresistive Effect

The magnetoresistive effect (MR Effect) is a condition in which the resistance of a conducting material changes in response to an applied magnetic field.[106] When an applied magnetic field is applied to an electrode material, the magnetic field changes the path of motion of the electrons within the material, resulting in a change in resistance. This mechanism of change is categorized into the following types: 1) Normal magnetoresistive effect: the resistance increases with increasing magnetic field. The reason for this is that the applied magnetic field deflects the trajectory of the electrons in the conductor, creating a helical motion, which increases the effective path length of the electrons, thus increasing the resistance.[107] 2) Giant magnetoresistive effect (GMR): In multilayer membrane structures, the resistance decreases significantly with the direction of the applied magnetic field. This effect is commonly used to study composite or nanostructured materials.[108] 3) Negative magnetoresistance effect: In some cases, the application of a magnetic field leads to a decrease in resistance, which is related to the spin correlation states of electrons and their interactions.[109]

This effect has an important influence on the electron transport properties and electrocatalytic performance in water electrolysis systems. During water electrolysis, the current passes through the electrodes to initiate redox reactions, and the electron transport behavior directly affects the rate and efficiency of the reactions. By adjusting the strength and direction of the applied magnetic field, the current distribution of the electrode can be optimized, the electron transfer path can be improved, and the catalytic performance of the electrode can be enhanced.[110] Modulation of electron transport behavior in water electrolysis reactions can be achieved by using magnetically responsive electrode materials or by applying an external magnetic field.[111] The magnetoresistive effect can change the conductivity of the electrode material and optimize the charge distribution on the electrode surface, making the electrochemical reaction more efficient. The study on the relationship between the magnetic resistance and overpotential of $Ni(OH)_2$, NiO, and Ni in constant magnetic fields of different sizes indicated that the decrease of overpotential showed a consistent change with the change of

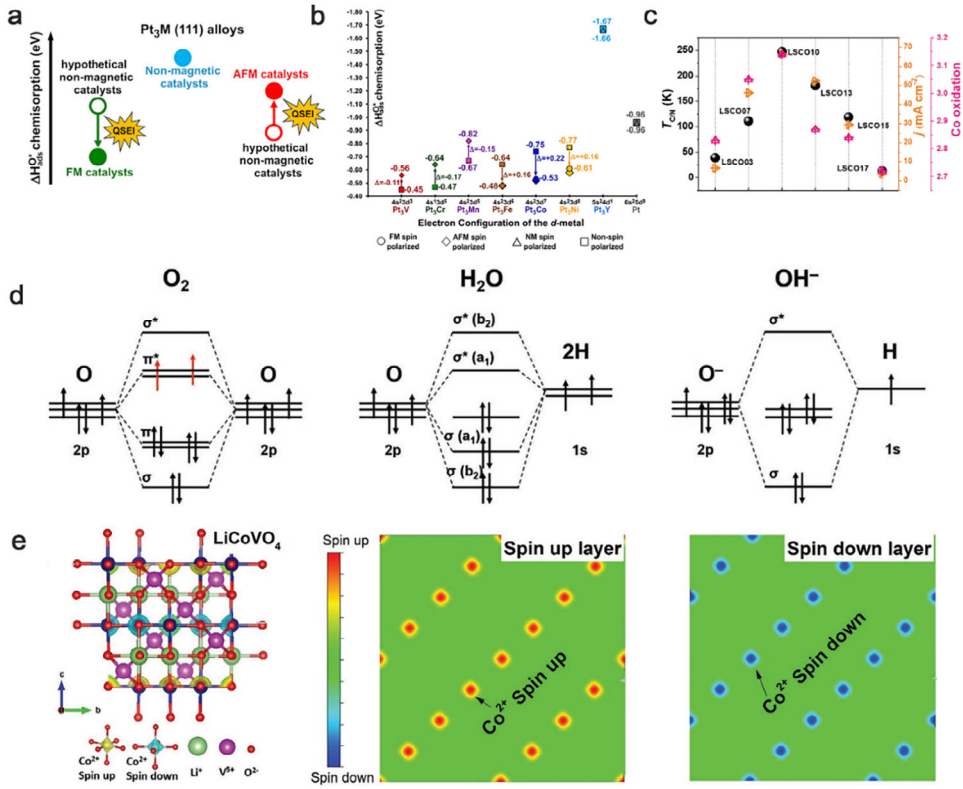

Figure 9. a) Role of quantum spin exchange interaction in the catalytic process; b) O* adsorption trends of Pt_3M (M = V, Cr, Mn, Fe, Co, Ni, Y) systems with different magnetic properties versus the metal d electronic configuration. Adapted with permission.[113] Copyright 2020, American Chemical Society. c) Volcano plot between Curiel temperature and properties of LSCO. Adapted with permission.[114] Copyright 2021, John Wiley and Sons. d) Electronic orbital structure of O_2 H_2O OH^-. Adapted with permission.[54] Copyright 2020, John Wiley and Sons. e) Spin density distribution of LiCoVO4. Adapted with permission.[115] Copyright 2020, John Wiley and Sons.

magnetoresistance. MR effect changed the electrical conductivity of the material itself and promoted the transfer of interfacial charge, which might be the dominant factor in the magnetic field-assisted OER process, and that the magnetically induced OER enhancement was most obvious in the negative MR effect of the catalysts is most obvious, and the overpotential at a current density of 10 mA cm^{-2} can be reduced by 20 mV under an applied magnetic field of 1.4 T.[29] In addition, J Jayeeta et al. achieved a current density and overpotential enhancement of 650% and 20%, respectively, after applying an external magnetic field of 300 mT to nanostructured floral carbon particles (NCFs) decorated with iron-paramagnetic nanoparticles (Co_3O_4, Co, and Ni-Co). A 22% decrease in magnetoresistance and 84.8% decrease in charge transfer resistance when a 100 mT magnetic field was applied resulted in a 2.5-fold increase in the hydrogen generation volume, and this enhancement originated from the magnetic field-induced decrease in magnetoresistance of the ferro-paramagnetic catalysts, as well as from the dynamic size expansion of the NCF-loaded catalysts.[112]

3.6. Electron Spin Selection

In addition to the magnetic enhancement effect mentioned above, the mechanism of the magnetic field's influence on the electronic structure of the active site is being studied more and more intensively. Jose Gracia et al. reveal a link between catalytic reactions and the catalyst's intrinsic ferromagnetism; antiferromagnetic quantum spin exchange interaction enhances interatomic electron Coulomb repulsion and localization, ferromagnetic quantum spin exchange attenuates electron repulsion and localization, and catalysts with ferromagnetism ordering can create a spin channel for the rapid transfer of spin-polarized electrons (**Figure 9**a,b).[113]

Bowl-mounted ferromagnetic MoS_2 synthesized by Wang et al. by designing nanostructures using gas-phase chemical deposition, improves electron-transfer efficiency under a magnetic field.[116] Compared with the layered MoS_2, the bowl-shaped MoS_2 has a narrower forbidden bandwidth because the symmetry of the upper and lower spins is broken, the unpaired spins are mainly concentrated on the edge Mo end faces, and the unsaturated coordination of the edge atoms leads to a certain magnetic moment of the bowl-mounted MoS_2. The bowl-mounted MoS_2 ferromagnetism leads to a greater sensitivity to external magnetic fields, and the electrons of MoS_2 have relatively high energies under the magnetic field, which makes it easier to jump to the active site and improves the efficiency of electron jumping. Chen et al. prepared NiMnIn alloy thin films by pulsed laser deposition, and the overpotential decreased by 8 mV under a magnetic field of 8000 Oe, suggesting that the magnetic field can

accelerate the transfer of electrons to the active site and the generation of intermediates under the effect of spin selection.[117] Cheng et al. established a simple Curie/Niel temperature as a new OER activity descriptor based on the inference that both catalyst magnetism and OER originate from electron exchange interactions, and the OER parameter is in high agreement with the electronic structure parameter and Curie-Niel temperature (Figure 9c).[114]

Catalytic reactions are closely related to the electronic configuration of the active site and reaction intermediates. In the field of oxygen electrocatalysis, the ground state of the oxygen molecule is a triplet state, with the front Π* orbitals occupied by two parallel-aligned electrons, in contrast to the spin state of OH^-/H_2O, which is a singlet state (Figure **9d**).[54] In the absence of an applied magnetic field, efforts have been made to modulate the spin state of the metal sites of the catalyst to achieve spin polarization and promote the generation of triplet oxygen molecules.[118] Xu et al. studied $LiCoVO_4$ with a layered antiferromagnetic anti-spinel structure, where the octahedral Co^{2+} has a spin-polarized channel, and the positive and negative magnetic moments of Co^{2+} ions in the oxide are arranged alternately with the layering so that the Co—O bonds along the magnetically polarized channel have a certain spin property, which can help to realize the catalytic pathway of the spin-polarization. Studies on antiferromagnetic $LiCoVO_4$ demonstrate that spin polarization can be achieved in antiferromagnetic catalysts in the absence of an external magnetic field. Ferromagnetism is a prerequisite for the realization of the spin-polarization effect of the magnetic field (Figure 9e). OER Some conventional descriptors, such as e_g-electron, ΔG_O-ΔG_{OH}, d-band centers, and charge-transfer energies, etc., are reasonable descriptors that can give a volcano-type relationship between the catalytic activity and the descriptors, which can help to find a highly active catalyst based on the volcano diagram.

José Ramón Galán-Mascarós et al. reported the improvement of OER efficiency under a magnetic field for a series of oxides with different magnetic properties and found that the magnetic enhancement tends to correlate positively with the magnetization intensity and that the magnetic field contributes to the parallel arrangement of oxygen radicals in the formation of O—O bonds under alkaline conditions (**Figure 10a**).[119] In the presence of a magnetic field, the spin alignment of the catalyst metal active site selectively transfers electrons in the reaction intermediates whose spin orientation is different from that of the active site, facilitating the generation of triplet O_2 with lower potential barriers. The activity of OER is proportional to the degree of interatomic ferromagnetic coupling, suggesting that the spin-selective charge mobility is directly correlated with the reactivity. The ordering of ferromagnetic orbitals in magnetic oxides helps to regulate the binding energy of reactants through quantum spin-exchange interactions. Zhang et al. altered the ratio of metal atoms of $Co_xNi_{1-x}Fe_2O_4$ to change the crystal structure and intrinsic magnetism of the catalysts, which affects the super-exchange between ions and the spin polarization under a magnetic field. It was demonstrated that the catalysts with different magnetization rates had different degrees of OER activity enhancement under the same magnetic field, and the OER activity enhancement of the samples increased with the increase of intrinsic magnetism.[120]

After the easily spin-polarized ferromagnetic exchange, the adsorbed O species will fix the spin direction, and the subsequent electron transfer according to Hand's rule and Pauling's incompatibility principle will be spontaneous spin-polarized, which ultimately leads to the generation of the triplet state O_2.[74] Additionally, according to the study of $LaSrMnO_3$, the magnetic field increases electron occupancy in the vicinity of the Fermi energy level, elevates the d-band center of Mn, and strengthens the adsorption of the reaction intermediates(Figure 10b–f).[121] This is consistent with previous studies that spin-polarized surfaces, due to increased electron occupation of the M-O bonding orbitals, exhibit stronger adsorption than non-spin-polarized surfaces.[124]

The changes in the structure of magnetic domains can be used to explain the improved activities under magnetic fields.[125] Magnetization leads to the evolution of the magnetic domain structure of the catalyst from a multi-domain to a single-domain structure, and the optimized path of OER spin promotion occurs on the surface where the domain junctions disappear (Figure 10g). It is found that single-domain catalysts exhibit similar OER increments as multi-domain catalysts in the absence of an external magnetic field, the intrinsic activity of single-domain catalysts is higher than that of multi-domain catalysts, and the magnetization effect promotes the approach of multi-domains to single-domains.[122] After the catalyst size is reduced to a single-domain structure, the spins are already aligned and spin polarization has theoretically already occurred; thus, single-domain catalysts do not require an external magnetic field to achieve spin-polarized performance. An external magnetic field is not necessary to improve the catalytic efficiency of the catalyst, and spin-polarization enhancement occurs as long as the ferromagnetic catalyst has a single domain structure.

However, Xu et al.'s study of single-domain $CoFe_2O_4$ showed that single-domain catalysts with high coercivity also assist in OER performance enhancement under the magnetic field. The size of single-domain particles, the ordering of magnetic permeability, and susceptibility to the magnetization direction of each magnetic domain particle (Figure 10h).[123] Xu et al. proposed that compared with the $CoFe_2O_4$ nanoparticles with low coercivity and high coercivity, the number of magnetic domains with different directions of easy magnetization distributed per unit volume is higher, and the orientation of the magnetic moments inside the material is relatively random; the magnetic domains of the material with high coercivity are relatively fewer, and the directions of easy magnetization tend to be parallel. For catalysts with single domains, the magnetization process involves only the rotation of the magnetic moments, and the spin-polarized state with higher coercivity facilitates the ferromagnetic ordering and can accelerate the electron transfer process.

The dissociation of the O-H bond during the OER process is affected by the external magnetic field.[126] The nucleophilic attack of H_2O on Fe = Od was demonstrated to be a step in the weakly basic OER reaction using phosphate modification of the Fe_3O_4 surface. Replacement of H_2O with D_2O confirms that the magnetic field-promoted spin-flip promotes O—H bond breaking under neutral or weakly alkaline PH conditions, acting in

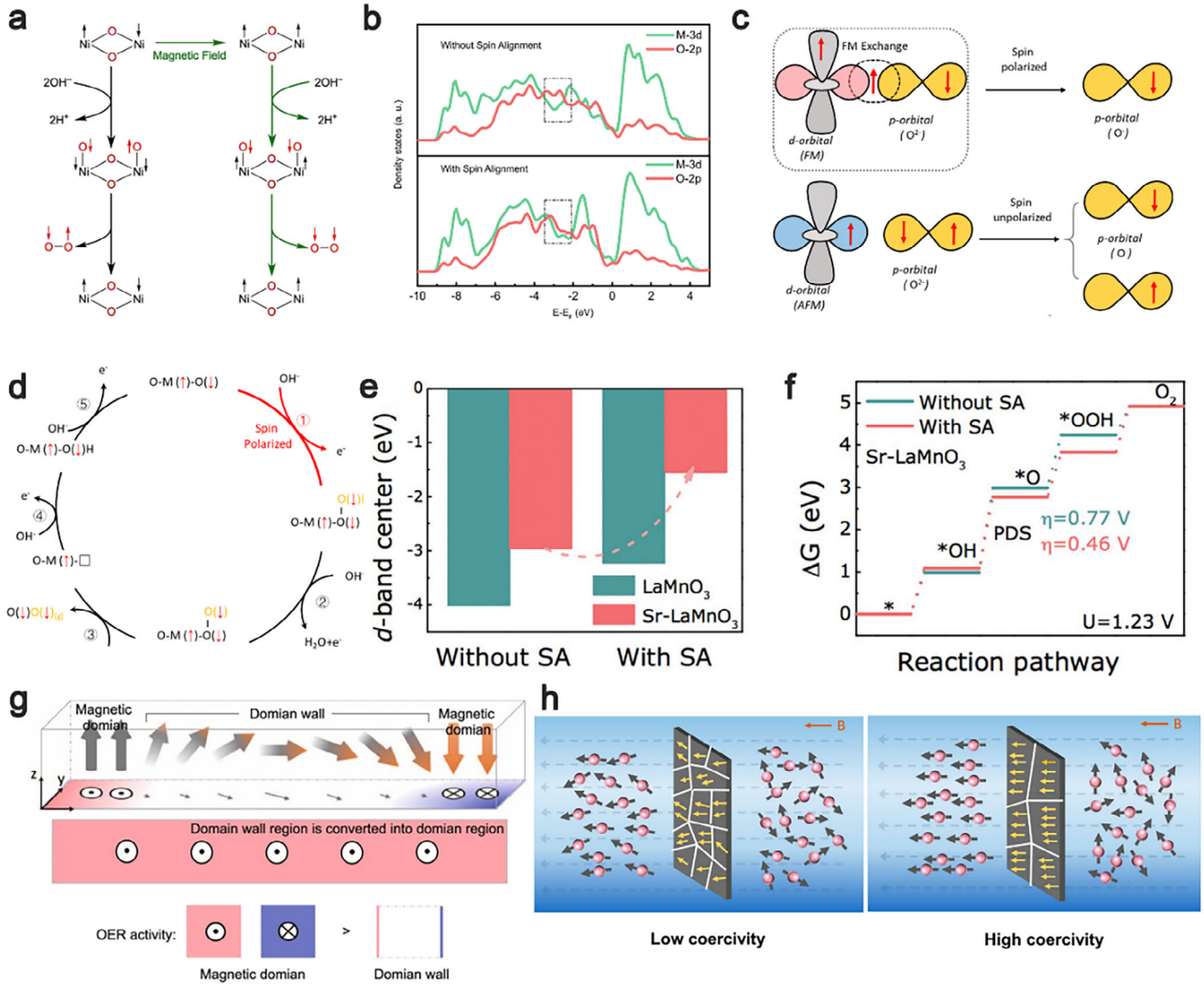

Figure 10. a) Spin antiparallel and spin polarization mechanisms of OER before and after the application of the magnetic field. Adapted with permission.[119] Copyright 2019, Springer Nature. b) The projected density of states (PDOS) of $CoFe_2O_4$ without and with spin alignment; c) Ferromagnetic exchange interaction of $CoFe_2O_4$ promotes spin-polarized electron transfer; d) OER path of spin-polarized electron transfer. Adapted with permission.[74] Copyright 2021, Springer Nature. e,f) Effect of spin polarization on d-band centers and Gibbs free energy. Adapted with permission.[121] Copyright 2023, John Wiley and Sons. g) Schematic diagrams of the magnetic domain structure and the domain walls of NiFe films with different thicknesses, and the arrows indicate the distribution of the magnetization strength. Adapted with permission.[122] Copyright 2023, Springer Nature. h) Spin-polarized electron transfer in CFOs with different coercivities. Adapted with permission.[123] Copyright 2022, American Chemical Society.

concert with the triplet state O-O bond, and that the magnetic current induced by the applied magnetic field is 20 times higher under weakly alkaline conditions (PH = 9, oxidation of the H_2O molecule) than the current under strongly alkaline environments (PH = 14, oxidation of OH). Previous studies on triplet O—O bonding have been applied only to O_2 generation, and the modulation of O—H or other bonds by magnetic fields extends the application of spin-catalytic strategies (**Figure 11a**).

Xue et al. showed that the alternating magnetic field can realize the transition from low to high spin state of octahedrally coordinated Fe in Fe_3O_4, and the OER overpotential is reduced by 66 mV at 10 mA cm^{-2}. The magnetic field can accelerate the transfer of unpaired electrons from the d orbitals as well as the reconstruction of FeOOH on the surface, and the generation energy of FeOOH in the high spin state (−62.596 eV) is less than that of the low spin state (−35.796 eV) (Figure 11b).[127] Ding et al. proposed a strategy to enhance the catalytic performance of bifunctional magnetocatalytic nanocages (MCNs) using a magnetic field. N, F, and B co-doped C nanofibers (PCNFs) loaded with Co nanodots with an average size of around 10 nm were obtained after electrostatic spinning and high-temperature pyrolysis. The interconnected nanocages in MCN have a limiting effect on the magnetic field, and the macropores in the material can act as electrostatic shielding, forming vortices to accelerate the electron leaps, promoting the transition of Co from low to high spin, generating more unpaired electrons in the 3d orbitals, and

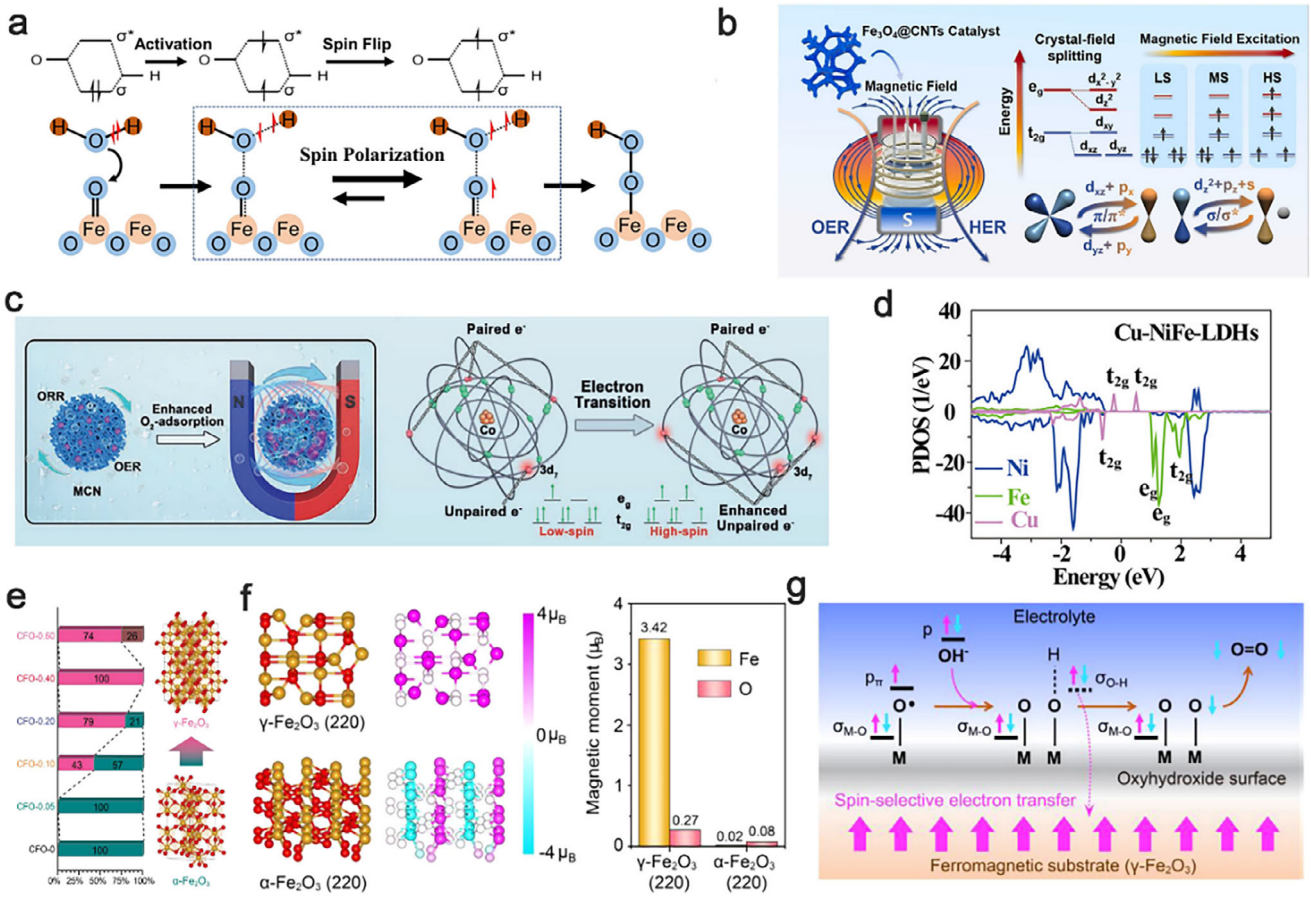

Figure 11. a) Spin-polarization mechanism of O—O bond coupling and O—H bond breaking during OER. Adapted with permission.[126] Copyright 2023, John Wiley and Sons. b) The magnetron regulation strategy enhances the hydrogen and oxygen evolution activity of Fe_3O_4@CNTs heterostructure. Adapted with permission.[127] Copyright 2024, Elsevier. c) Schematic of magnetically enhanced OER and ORR. Electron jump of Co from low to high spin. Adapted with permission.[128] Copyright 2020, John Wiley and Sons. d) PDOS of Cu^{2+}-doped NiFe-LDHs. Adapted with permission.[129] Copyright 2022, American Chemical Society. e) Co content modulates the phase transition of Fe_2O_3; f) magnetic moment distribution of different phases of Fe_2O_3. g) Schematic illustration of spin-selective electron transfer into the ferromagnetic substrate (γ-Fe_2O_3). Adapted with permission.[130] Copyright 2024, American Chemical Society.

efficiently enhancing the adsorption of oxygen intermediates and the four-electron transfer process of ORR and OER (Figure 11c).[128]

The above studies are directed at ferromagnetic catalysts, and some catalysts with excellent properties (sulfides, hydroxides, single atoms, etc.) tend to exhibit paramagnetism or antiferromagnetism and are insensitive to magnetic field response. Layered bimetallic hydroxides due to antiferromagnetic interactions between M-OH-M,[131] LDHs are usually low-temperature ferromagnets, based on the paramagnetism of NiFe-LDHs, the introduction of heteroatoms into LDHs can regulate the spin state of metal ions through electronic coupling effects, Sun et al. synthesized Cu^{2+}-doped NiFe-LDHs nanosheets, the introduction of Cu^{2+} led to the mismatch of the original metal ion ligand polyhedra, which altered the proximity charge distributions and the electronic spin states, and the calculations showed that the Cu^{2+}-induced Jahn-Teller effect promotes the splitting of the spin state of Fe^{3+} and realizes the transition of NiFe-LDHs to ferromagnetism, which has a positive effect on the formation of O—O bonds and the magnetic field accelerates the generation of paramagnetic oxygen molecules from antiferromagnetic substances (Figure 11d).[129] α-Fe_2O_3 usually exhibits antiferromagnetism. Song et al. used Co to modulate the phase transition from α-Fe_2O_3 to β-Fe_2O_3 to achieve the transition to ferromagnetism, and the CFO-0.2 overpotential was reduced by 10 mV under a magnetic field of 200 mT and a current density of 100 mA cm^{-2}. The O atoms in β-Fe_2O_3 have an effective magnetic moment of 0.27 μB due to the spin-polarized spillover of the metal cations. has an effective magnetic moment of 0.27 μB, and the same spin configuration of the metal and oxygen atoms provides a spin conduction channel for the transfer of spin electrons during the OER process (Figure 11e–g).[130]

Lu et al. designed Ni@MoS_2 with a high-density atomic dispersion with short-range quantum spin-exchange interactions and long-range ferromagnetically ordered active centers, the high metal doping density reduces the average spacing between adjacent magnetically doped sites, leading to the transformation of the interatomic magnetic exchange interactions into ferromagnetism ordering, and the fact that Ni and MoS_2 are a twisted tetragonal structure promotes ferromagnetism between Ni and

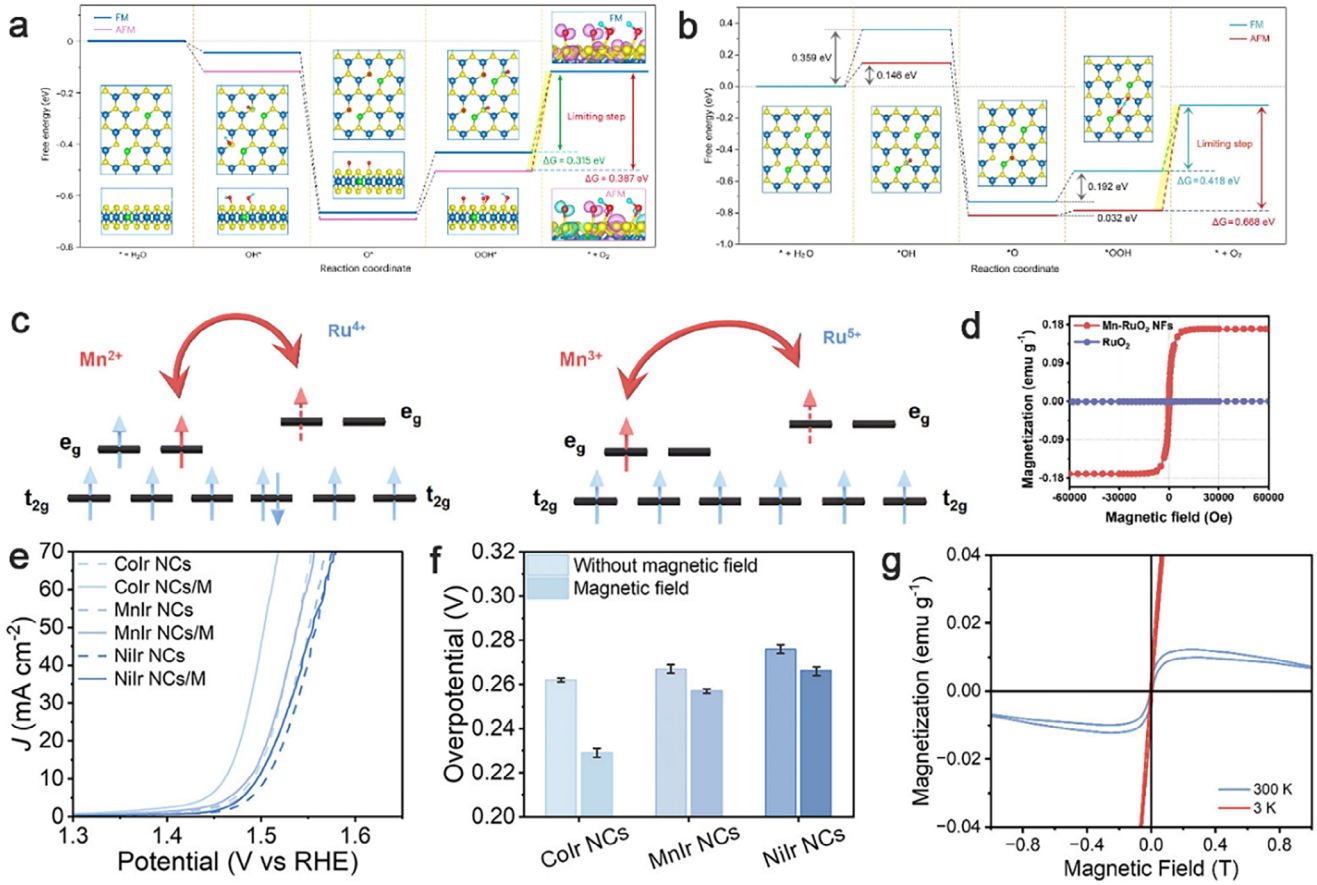

Figure 12. a,b) OER adsorption of oxygen and Gibbs free energy changes of O—H—O bridging mechanism for Ni/MoS_2 SACS in ferromagnetic and antiferromagnetic configurations. Adapted with permission.[132] Copyright 2023, Springer Nature. c) Schematic of the ferromagnetic exchange between Mn and Ru; d) Variation of OER properties of Mn-doped RuO_2 under a magnetic field. Adapted with permission.[133] Copyright 2023, John Wiley and Sons. e,f) Variation of OER properties of CoIr/MnIr/NiIr alloys under magnetic field; g) M-H curves of CoIr/MnIr/NiIr alloys. Adapted with permission.[134] Copyright 2024, American Chemical Society.

the adjacent S coupling, leading to room temperature ferromagnetism. The magnetic field enhancement is attributed to the magnetic field-induced hybridization of the p-d orbitals of S-Ni, which in turn induces the optimization of the spin alignment of the S site and the spin density of the S active center. The intermediates adsorbed on the S sites in the ferromagnetic configuration show a spin-parallel arrangement, and an antiparallel arrangement in the antiferromagnetic configuration, with the parallel arrangement favoring OOH desorption (**Figure** 12a,b).[132]

Currently, commercially available catalysts are dominated by RuO_2 and IrO_2, which have high activity in acidic media. However, they usually exhibit antiferromagnetism and do not have the possibility of magnetic field enhancement. Shao et al. addressed the magnetic as well as OER properties of noble metal catalysts by introducing Mn, which has a pronounced Jahn-Teller effect, into RuO_2, and the super-exchange interaction between the localized spin state of Mn and the antiferromagnetic RuO_2 led to ferromagnetism and the reduction of the OER overpotential at 10 mA cm^{-2} by 57 mV under a magnetic field of 330 mT (Figure 12c,d).[133] Ir is a non-magnetic metal, the same as RuO_2 also impossible to use for magnetic field enhancement OER.[134] Shao et al. used the exchange interaction between 3d metal (Co/Mn/Ni) and 5d metal atoms (Ir) to convert it into a ferromagnetically ordered metal, CoIr alloy has the highest spin-polarization strength, and the overpotential decreases by 40 mV under a magnetic field (Figure 12e–g).

3.7. Spin Pinning Effect

Spin pinning effect refers to the phenomenon where the spin direction of electrons is fixed at certain interfaces or defects, making it difficult to change. This phenomenon usually occurs at ferromagnetic/non-magnetic interfaces or ferromagnetic/antiferromagnetic interfaces. Modulation of catalyst magnetism by doping, structural phase modulation, or construction of ferromagnetic/paramagnetic and ferromagnetic/antiferromagnetic interfaces and heterojunctions is another strategy to achieve magnetic field enhancement. During the OER process, most of the catalyst surfaces undergo remodeling to generate a more active hydroxyl oxide catalytic layer, but the hydroxyl oxides usually exhibit nonferromagnetism.[135,136] Cr_2Te_3 through proximity to antiferromagnetic (AFM) CrOOH,

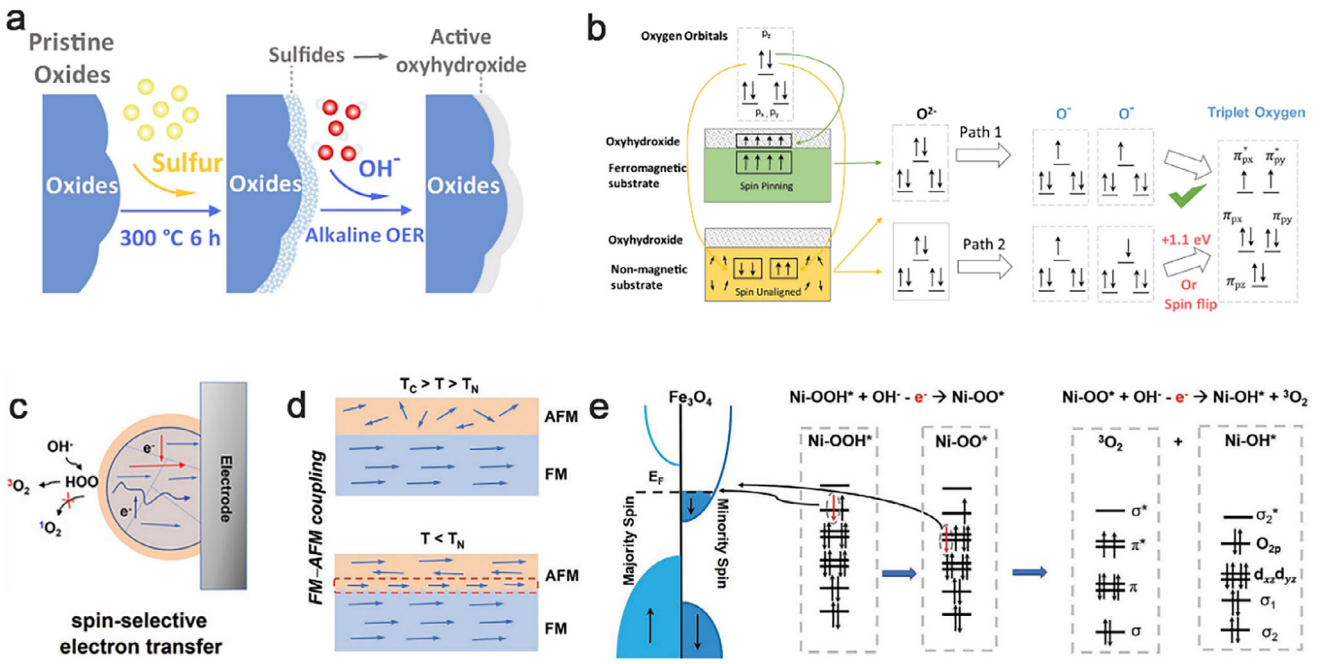

Figure 13. a) The schematic diagram of a controllable reconstruction on oxides by controlling the sulfurization; b) Spin-polarized electron transfer due to spin pinning effect; Adapted with permission.[138] Copyright 2021, Springer Nature. c) Scheme illustration of spin-selective electron transport OER mechanism; d) Schematic diagram of ferromagnetic-antiferromagnetic coupling; e) Spin-selective electron transfer mechanism in core–shell nanoparticles. Adapted with permission.[139] Copyright 2021, John Wiley and Sons.

which results in long-range ferromagnetic ordering, realizing room-temperature ferromagnetism due to the presence of magnetic proximity effects at the PM/AFM interface, and spin-related OER dynamics are present at the interface.[137] The spin-nailing effect is achieved at the MO/MOOH interface by precisely regulating the surface remodeling of ferromagnetic oxides, which is attributed to the strong magnetic anisotropy field induced by robust chemical bonding at the interface between ferromagnetic and paramagnetic materials (**Figure 13**a,b).[138] The FM-AFM Fe_3O_4@$Ni(OH)_2$ core-shell catalysts designed by Xu et al. resulted in the selective removal of spin-polarized electrons due to the interfacial coupling under the magnetic field, and the interfacial coupling effect can be efficiently maintained when the thickness of the catalyst's shell layer is small. The strong coupling effect can lead to a spin-polarized surface. Moreover, the core magnetic domain structure was regulated by controlling the particle size, and the magnetic field had a greater effect on the catalytic activity when the core was a multi-domain structure(Figure 13c,d).[139] Under the influence of the spin-pinning effect, the paramagnetic hydroxyl oxide on the surface carries out the transfer of spin-polarized electrons in the catalytic reaction and improves the efficiency of the catalytic reaction (Figure 13e).

Under the magnetoresistance effect and the penetration effect of the ferromagnetic exchange field, the spin-polarized electron transport across the grain boundaries has a great influence on the material resistance, and the alignment of adjacent grain boundaries improves the degree of electron tunneling across the boundaries and reduces the electrical resistance, and due to the penetration effect of the ferromagnetic exchange field, the non-ferromagnetic Mo- NiS_x exhibits magnetic activity and thus spin polarization, so the magnetic field improves the performance of HER and OER.[140] The application of Mo-NiS_x/NF to construct a water electrolyzer achieved a low voltage of 1.594 V, providing a new way to realize the spin-polarization effect in non-ferromagnetic catalysts. The Fermi energy level difference of the P-N junction causes the redistribution of electrons at the non-homogeneous interfaces, and the transfer of spin-polarized electrons is accelerated due to the exchange bias effect between the magnetic substrate (NF) and the surface active material, the spin-polarization due to the ferromagnetic-antiferromagnetic coupling between the interfaces and the magneto-resistive effect induced by the parallel arrangement of the magnetic moments of the atoms. The study on NiFe-LDHs/Co_3O_4/NF indicated that the combined effect of electronic modulation and magnetic field is an effective method for designing efficient magnetized catalysts.[141]

3.8. Magnetic Field Induced Structural Reconstruction

In addition to magnetic field modulation of electron spin, Huang and Kan et al. found that the tetrahedral and octahedral units of spinel oxides can be modulated by a magnetic field.[142] It is shown that mixed spinel $NiFe_2O_4$ is forced to migrate Ni^{2+} from octahedral to tetrahedral sites under the influence of a large magnetic field, leading to an increase in the number of tetrahedral sites exposed to the surface, and DFT calculations show that the catalytic activity of Ni^{2+} located in the tetrahedral sites of the surface is superior to that of the octahedral sites, which when coupled with the magnetohydrodynamic effect of the magnetic field as well as the spin-selectivity, results in the realization of an excellent OER activity. Huang et al. explain that the magnetic field induces the transfer of Ni^{2+} from the octahedral to the tetrahedral

position; however, the magnetic field may not directly lead to the migration of the ionic coordination position. A recent study by Wong et al. revealed that Cr^{3+} in CrO_6 octahedra is oxidized to Cr^{6+} to become tetrahedrally coordinated,[143] perhaps possibly due to the effect of the magnetic field on the magnetic structure of the oxide, leading to a change in the oxidation state of Ni, ultimately leading to a change in the coordination environment. A recent study by Wong et al. revealed that Cr^{3+} in CrO_6 octahedra is oxidized to Cr^{6+}, changing to tetrahedral coordination, perhaps possibly due to the effect of the magnetic field on the magnetic structure of the oxide, leading to a change in the oxidation state of Ni, ultimately leading to a change in the coordination environment.

The strain induced by magnetostriction can also lead to changes in water electrolysis behavior. To investigate the influence of magnetic fields on oxygen evolution reactions in FeCo alloys with different phase structures, Liu et al. synthesized alloy catalysts with bcc, fcc, and bcc+fcc phase structures by adjusting the ratio of Fe and Co elements.[37] Under the influence of a magnetic field, magnetostriction occurs in the FeCo alloys, generating strain within the material. This strain modifies the d-band center of the metals, thereby promoting the adsorption of reaction intermediates. Alloys with different phase structures exhibit varying magnetostrictive properties, and the study reveals that the magnetic field enhancement effect is proportional to the magnetostrictive performance.

4. Magnetic Fields Sensitive Materials

In current research progress, a majority of electrocatalytic materials for water splitting are transition metals and their compounds, primarily including alloys, metal oxides, metal hydroxides, metal sulfides, and metal phosphides. These catalytic materials exhibit diverse magnetic properties, which can be categorized into ferromagnetic, antiferromagnetic, paramagnetic, and superparamagnetic materials, as well as topological magnetic materials and composite magnetic materials. This chapter focuses on several materials with unique magnetic and catalytic properties, which are expected to demonstrate excellent performance and stability in the process of magnetic field-coupled water electrolysis. These findings also provide valuable references for the design of magnetically sensitive materials.

4.1. Amorphous Alloy Materials

In recent years, amorphous transition metal compounds have demonstrated excellent electrocatalytic performance due to their abundant active sites, high surface energy, and superior corrosion resistance.[144–146] At the atomic level, these materials exhibit long-range disorder and short-range ordered atomic cluster structures, which result in numerous dangling bonds or coordinatively unsaturated atoms on the surface, providing a higher density of active sites for catalytic reactions.[147] This unique atomic structure also induces significant local internal stress, leading to higher free energy and metastable states compared to crystalline materials.[148] These characteristics influence the electronic structure of catalytic active sites, thereby modulating the adsorption/desorption behavior of molecules and primary reaction intermediates, offering greater possibilities for tuning catalytic activity.[149] The absence of grain boundaries in amorphous alloys enhances their corrosion resistance and reduces pinning effects during magnetic domain movement, resulting in exceptional soft magnetic properties, including high saturation magnetization, low coercivity, high magnetic permeability, and low hysteresis loss.[150–153] These characteristics, particularly the excellent soft magnetic properties, make amorphous materials more susceptible to external magnetic fields, thereby facilitating spin polarization. This also renders amorphous materials an ideal choice for magnetic field-enhanced catalysts.

Crystallization and relaxation are inherent characteristics of the metastable state of amorphous alloys.[154] However, the interaction between these two processes is not yet fully understood. Song et al. discovered that amorphous materials at different enthalpy levels exhibit significantly different resistances to crystallization.[155] These findings provide new evidence for the heredity between glasses and liquids, suggesting that modulating the glassy state is a new way to control the crystallization kinetics of supercooled liquids. Additionally, high-precision nanocalorimetry revealed exponential relaxation events during the relaxation process, applicable to both metallic and organic glasses. The relaxation peaks can be well-fitted by an exponential Debye function with a single activation energy, covering a broad range from α-relaxation to β-relaxation and even rapid γ/β'-relaxation. These results provide a reliable theoretical foundation for precisely modulating the energy state and electronic structure of amorphous alloys.

Dealloying of amorphous alloys can form active porous structures/magnetic matrix self-supported catalysts. Amorphous alloys, due to their extremely high specific strength, elastic strain, and fracture toughness, are very suitable precursor alloys, providing an excellent foundation for the subsequent processing and application of dealloyed catalyst materials. We successfully prepared self-supported catalysts integrated with active nanoporous platinum/iron-based amorphous alloy matrix through dealloying, showing very high activity for hydrogen evolution, requiring only 102 mV overpotential at 1000 mA cm^{-2}, with Faradaic efficiency close to 100%.[156] This allows the current density to be increased to 500 mA cm^{-2} during stability testing without corrosion and degradation (**Figure 14a–c**).

Component tuning of amorphous alloys is one of the important means to influence catalytic activity, especially for multi-component alloys, mainly by modulating the electronic structure of active sites through the synergistic action of different elements to affect intrinsic activity. However, due to the multitude of element types and the difficulty in enumerating their proportions, determining the best composition of catalysts is challenging both computationally and experimentally. We proposed a scalable high-throughput bubble screening method to identify multi-component alloys with the highest catalytic performance.[157] As proof, this method identified the optimal composition in ternary Ni–Co–Ti and Ni—Fe–Au alloys with superior intrinsic catalytic activity. Single electrochemical tests further confirmed the advanced catalytic performance of the best $Ni_{56.5}Co_{35}Ti_{8.5}$ alloy band, with an overpotential of about 425 mV at 500 mA cm^{-2} and a Tafel slope of about 82 mV dec^{-1}. This is attributed to low atomic packing density and low electronic binding energy. The scalable high-throughput strategy introduced is not only limited

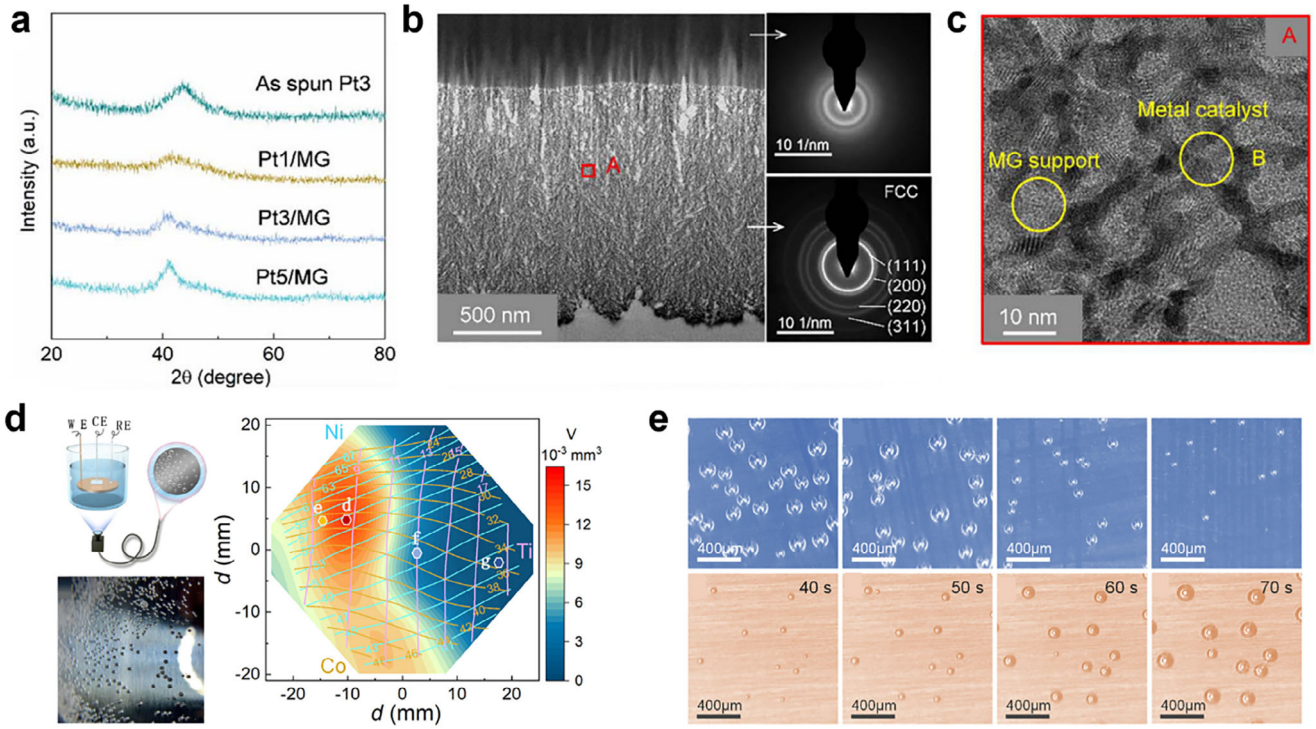

Figure 14. a–c) Structural characterization of Pt/MG catalysts; Adapted with permission.[156] Copyright 2024, Royal Society of Chemistry. d,e) Schematic of high-throughput screening for HER by monitoring bubbles using a camera. Adapted with permission.[157] Copyright 2022, American Chemical Society.

to ternary catalysts for HER but also shows potential for exploring catalysts in higher component alloy systems (Figure 14d–e).

The design of crystalline/amorphous heterostructures has emerged as a groundbreaking strategy to optimize electrocatalytic performance, particularly for OER. By utilizing the unique advantages of amorphous alloys, such as disordered atomic arrangement, flexibility, and suppressed atomic migration, it is possible to construct heterogeneous interfaces in a controllable manner.[158] In the study by Li et al., FeNi-based alloy fibers with tailored N/A interfaces were synthesized via a melt-extraction method, where the cooling rate precisely controlled nanocrystal size within an amorphous matrix.[159] Key to this innovation is the introduction of nanocrystals (3–40 nm) into the amorphous framework, creating interfaces with "stepped surfaces" rich in high-energy atoms and unsaturated coordination sites. These interfaces significantly reduced the Gibbs free energy barrier for the rate-determining step ($\Delta G_{max} \approx 0.047$ eV), outperforming pure crystalline or amorphous phases. Experimental results demonstrated exceptional OER performance: a low overpotential of 227 mV @10 mA $\mathbf{cm}^{-2}$, a Tafel slope of 35 mV dec^{-1}, and unprecedented stability at industrial current densities (1000 h @ 500 mA cm^{-2}).

The preparation of amorphous alloy catalyst materials usually requires rapid cooling from the melt and deposition from the vapor phase, such as evaporation, ion sputtering, and glow discharge. Liquid-phase laser ablation can also provide conditions for preparing amorphous catalysts.[160] We successfully prepared amorphous iron-cobalt-nickel-based multimetal oxide $(FCNMA)O_x$ using liquid-phase laser ablation as a catalyst. Under an alternating magnetic field at 100 mA cm^{-2} current density, the overpotential decreased from 332 to 288 mV, mainly due to electron transfer between nickel and aluminum elements caused by the magnetic field, thereby increasing the ability of nickel elements as active sites to adsorb oxygen intermediates.

4.2. Topological Materials

Topological materials, due to their unique physical properties, are used to explore the interplay between surface states, electron transport, and surface catalytic reactions.[161] Topological semimetals, such as Weyl semimetals and topological nodal-line semimetals, provide a solid foundation for being potential high-efficiency catalytic platforms due to their ultra-high electron mobility, unique topologically protected surface states, robustness, and high electron state density.[162–164] Certain magnetic Weyl semimetals exhibit special magnetic properties such as the anomalous Hall effect, nonlinear magnetic transport phenomena, topological surface state Fermi arcs, and chiral anomaly negative magnetoresistance, and due to the breaking of time-reversal symmetry, they are easily manipulated and modulated by temperature or magnetic fields, making topological semimetal catalysts show significant potential and advantage in the field of magnetic field-enhanced electrocatalysis.[165]

Topologically protected surface states (TSS), arising from bulk band inversion, are non-trivial electronic states localized at material surfaces. These states exhibit robustness against surface modifications and defects, making them resistant to local perturbations. For example, $Co_3Sn_2S_2$ single crystals, which

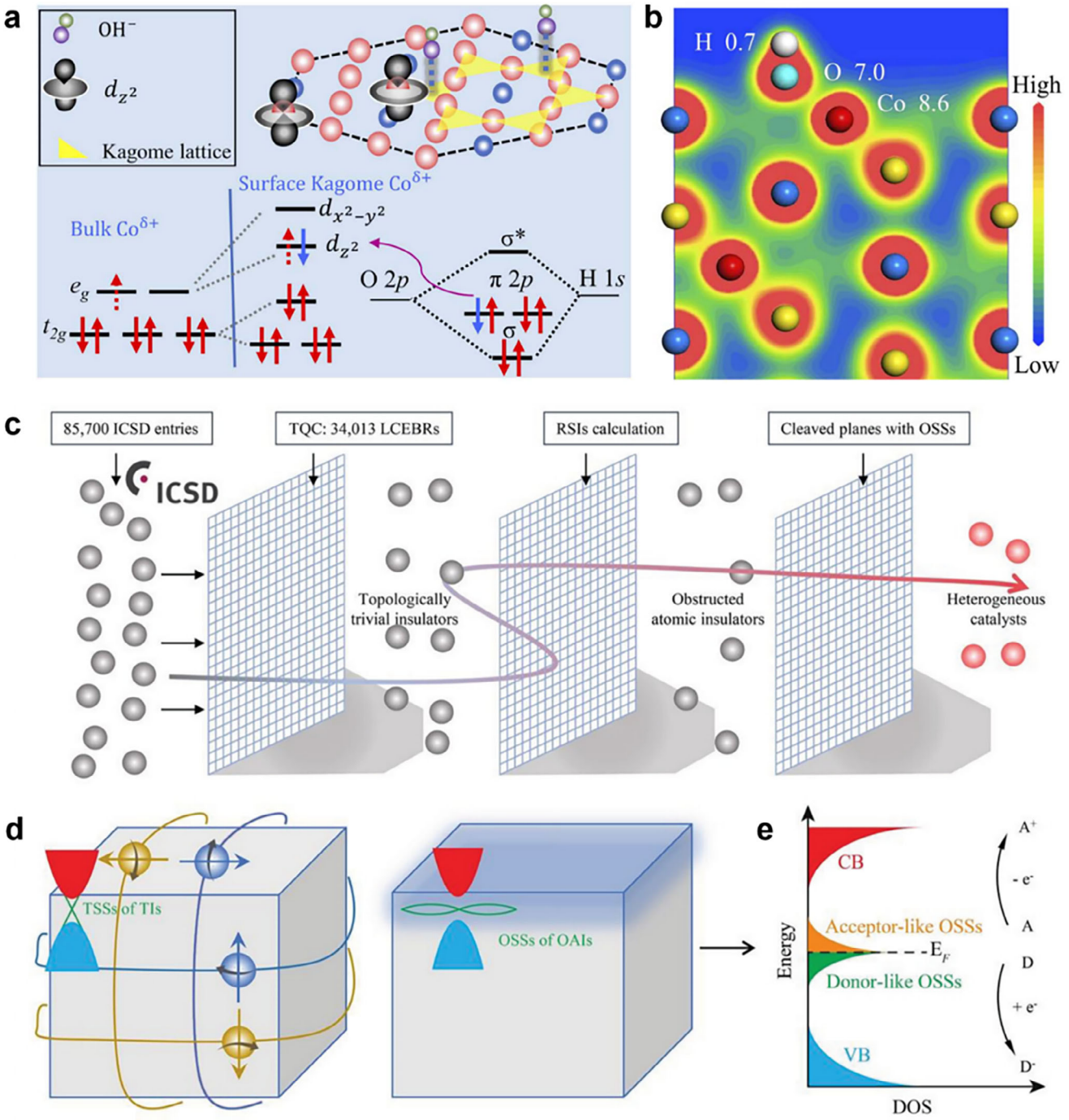

Figure 15. a) Schematic diagram of the favorable absorption of OH by Co 3d orbitals. b) The contour map of the total charge distribution of Co3Sn2S2 single crystal; Adapted with permission.[166] Copyright 2019, American Association for the Advancement of Science. c) Screening of potential OAIs and heterogeneous catalysts from the Topological Materials Database website by calculating the RSIs. d) Comparisons between the TSSs and OSSs. e) Illustration of the role of OSSs in OAIs for reduction and oxidation catalytic reactions. Adapted with permission.[167] Copyright 2022, John Wiley and Sons.

possess a topological semimetal band structure, demonstrate exceptional OER catalytic performance due to cobalt-derived surface states near the Fermi level, despite having a much smaller surface area compared to cobalt-based nanostructured catalysts. Experimental and theoretical calculations reveal that the partially filled e_g orbitals of surface Co atoms in $Co_3Sn_2S_2$ facilitate electron transfer and enhance the binding between adsorbates and catalytic sites (**Figure 15**a,b).[166] This finding offers a novel strategy for designing highly efficient OER electrocatalysts.

Many of the most advanced catalysts (such as Pt, Pd, IrO_2, and RuO_2) are theoretically or experimentally considered to have topologically derived surface states. These states are mainly composed of highly delocalized s_p orbitals (noble metals) or d orbitals with strong spin-orbit coupling (noble metal oxides). The identification of obstructed atomic insulators (OAIs) featuring crystal symmetry-protected metallic surface states enables the precise determination of catalytically active sites within inorganic crystalline materials.[167] The obstructed Wannier charge centers (OWCCs) in these OAIs are symmetry-fixed at certain empty Wyckoff positions, thus ensuring that surfaces accommodating these sites have metal obstructed surface states (OSSs). Our studies have shown that OSSs are the origin of catalytic activity in crystal materials. The consistency between OSSs and catalytic active sites has been theoretically verified in materials such as 2H-$MoTe_2$, 1T′-$MoTe_2$, and $NiPS_3$. In addition, the study successfully identified several efficient catalysts by considering the number and symmetry of OWCCs. By applying real-space invariant theory to a database of 34,013 topologically trivial insulators, 1,788 unique OAIs were identified, of which 465 may be high-performance catalysts (Figure 15c–e). This new method will promote and accelerate the discovery of new catalysts for a wide range of heterogeneous redox reactions.

Dirac node arc semimetals have Dirac nodes in their electronic band structure that connect the conduction and valence bands, as well as Dirac node arcs formed between these nodes, with linear dispersion relationships and high electron mobility. PtSn4 has excellent electrical conductivity, carrier mobility, and appropriate Gibbs free energy, which makes it perform well in HER. Studies found that the turnover frequency (TOF) of $PtSn_4$ is 1.54 H_2s^{-1}, setting a new benchmark among Pt-based noble metals and earth-abundant metal catalysts.[168] The surface states of $PtSn_4$ are stable and can effectively transfer electrons to adsorbed hydrogen atoms, thereby improving catalytic efficiency. In addition, $PtSn_4$ shows excellent chemical and electrochemical stability after long-term exposure to air and during prolonged HER stability tests. Fu et al. found that $PtSn_4$ shows strong longitudinal and transverse thermoelectric responses under a magnetic field. At about 15K, a large power factor and Nernst power factor of about 80–100 μW cm^{-1} K^{-2} were obtained, leading to a thermoelectric merit that is more than 30 times enhanced compared to no magnetic field. Through magnetic field modulation, $PtSn_4$ shows a significant enhancement in thermoelectric performance.

4.3. Ferrites and Metal Oxides

Ferrites, also known as ferrimagnetic or ferrite magnetic materials, are a class of ceramic materials with ferromagnetism, primarily composed of iron ions and other metal ions along with oxygen ions.[169] These materials typically possess specific crystal structures, such as spinel ($MgFe_2O_4$ e.g.,) and garnet structures ($Y_3Fe_5O_{12}$ e.g.,). These structures consist of cubic close-packed or hexagonal close-packed frameworks formed by oxygen ions, with metal ions filling the interstices.[170] The flexible positions and valence variability of metal cations endow spinel ferrites with diverse physicochemical properties, such as abundant surface active sites, high catalytic activity, and ease of modification through doping, surface modification, and structural control.[171] Additionally, the unpaired electrons of metal ions in ferrites provide the magnetic moments required for ferromagnetism, which offers potential for further study on the enhancement of ferrite catalytic materials under magnetic fields.

Doping is an effective method to alter the properties of materials by introducing other elements into ferrite materials, significantly affecting their physicochemical properties and optimizing their performance. Hassan et al.[172] successfully synthesized selenium-doped nickel ferrite ($NiFe_2O_4$, abbreviated as NFO) nanoparticles using pulsed laser ablation in liquid (PLAL). The results showed that all samples presented a single-phase structure, and the incorporation of selenium confirmed its presence in the spinel structure. Magnetic studies indicated that all selenium-doped NFO samples exhibited superparamagnetic at room temperature and ferromagnetism at 10K. Notably, when the selenium content reached 2%, the sample's magnetization significantly increased by about 20%. In terms of electrocatalytic, NFO+2%Se nanoparticles demonstrated excellent performance, with an HER overpotential 86 mV lower than that of undoped NFO. The performance enhancement was attributed to improved electrical conductivity and the nanosheet structure introduced by selenium doping, providing more active sites and surface area for catalytic water splitting.

Designing defects in the lattice, such as oxygen vacancies, can optimize the electronic structure and surface properties of materials, enhancing their electrochemical performance. Debnath et al.[173] synthesized oxygen-deficient cobalt ferrite ($CoFe_2O_4$) nanoparticles with rich oxygen defects through a co-precipitation method, controlling the quantity of oxygen defects by varying particle sizes, which in turn altered the catalyst's electronic structure and improved the adsorption-desorption kinetics of reaction intermediates. Among them, 20 nm (CoF-2) and 50 nm (CoF-3) served as excellent catalysts for HER and OER, respectively, with CoF-2 showing low overpotentials across different pH values, and CoF-3 requiring only 253 mV overpotential to achieve 10 mA cm^{-2} current density. In overall water splitting, the combination of CoF-3 and CoF-2 only needed a cell voltage of 1.63 V to reach 10 mA cm^{-2}, demonstrating good stability. By regulating oxygen defects, the electrocatalytic performance of spinel catalysts can be effectively improved, offering new insights for the development of efficient, low-cost water electrolysis catalysts.

Doping can also alter the particle size of ferrite catalysts, thereby affecting their magnetic properties and domain structure.[174] We synthesized $NZFO_x$ catalysts with varying zinc doping levels through a hydrothermal process. Changes in zinc doping levels led to variations in the strength of M-O-M super exchange interactions, affecting the spin directions of metal ions in octahedral and tetrahedral coordination, ultimately manifesting as changes in macroscopic magnetization. Zinc doping increased the formation energy of the system, reduced catalyst particle size, and transformed the structure from multi-domain to single domain. The change in catalytic performance under a magnetic field was consistent with the trends in magnetic domain structure and magnetic properties. Due to the evolution of magnetic domain structure under a magnetic field, multi-domain NFO exhibited the most significant changes under a magnetic field, with the alignment of domain walls under a magnetic field

being the main reason for the enhancement of catalytic performance. The single-domain structure experienced a slight energy state enhancement of catalytic active sites under a magnetic field, leading to improved catalytic activity, and the change amplitude gradually increased with the enhancement of magnetism.

4.4. Layered Double Hydroxide

The layered structure of LDH materials consists of positively charged metal hydroxide layers and intercalated anions and water molecules, endowing LDH with high tunability and customizability.[175] This structure not only endows LDH with excellent electrochemical activity and good conductivity but also provides abundant active sites and rapid charge transfer pathways during catalysis.[176] For instance, NiFe-LDH, containing magnetic metal ions, may alter its electronic structure and charge distribution under the influence of a magnetic field, thereby enhancing its adsorption capacity and catalytic activity towards water molecules.

Doping can introduce microstructures such as dislocations and stacking faults, optimizing the electronic states of LDH and increasing active sites, thereby enhancing its catalytic activity. Ye et al.[177] synthesized cobalt-doped nickel-iron layered double hydroxides as electrocatalysts for efficient overall water splitting. $Co_{0.03}$-$NiFe_{0.97}$ LDH demonstrated excellent electrocatalytic performance with overpotentials of only 170 mV (10 mA cm^{-2}) for HER and 280 mV (50 mA cm^{-2}) for OER in alkaline solutions. Under industrial conditions, the electrocatalytic activity of $Co_{0.03}$-$NiFe_{0.97}$ LDH was superior to commercial Raney nickel and Pt/C||IrO_2. The study improved the activity of overall water splitting catalysts by introducing microstructures. We regulated the d-orbital hybridization of Ni in NiFe LDH by introducing heteroatoms Al, thereby adjusting p-d orbital coupling and significantly altering the electronic structure and geometric configuration of the material. This change was beneficial for adjusting the electron distribution on the e_g and t_{2g} orbitals of active atomic centers. At a current density of 50 mA cm^{-2}, the overpotential of NiFeAl LDH-M decreased by 28 mV when a 600 mT magnetic field was applied compared to when no magnetic field was applied. According to molecular orbital theory, the spin-Ni atoms adsorbing OOH* have empty or half-filled d orbitals, leading to a higher bond order and thus enhanced adsorption capacity for oxygen intermediates, improving OER performance.

Constructing heterointerfaces is a strategy that can effectively modulate the electronic structure and optimize the surface properties of electrode materials.[178] Wang et al.[179] synthesized a heterostructure of CuNi alloy and CoFe LDH in situ on nickel foam through a two-step electrodeposition process, serving as an efficient bifunctional electrocatalyst for overall water splitting. The synergy between the CuNi alloy and CoFe LDH optimized the interfacial electron distribution, significantly enhancing the intrinsic activity of the HER and OER. The optimal CuNi/CoFe LDH@NF bifunctional catalyst exhibited extremely low overpotentials in alkaline electrolyte, with 56 mV for HER (10 mA cm^{-2}) and 268 mV for OER (50 mA cm^{-2}), and only required a low cell voltage of 1.49 V to achieve 10 mA cm^{-2} in overall water splitting. Density functional theory calculations indicated that constructing heterojunction interfaces promoted the redistribution of interface electrons and optimized the free energy of adsorbed intermediates, thereby reducing the energy barrier of the rate-determining step (**Figure 16**a,b). Overall, the influence of magnetic fields on LDH material performance is complex and requires detailed analysis through experimental studies and theoretical simulations, offering new possibilities for improving electrolysis efficiency and reducing energy consumption.

4.5. Single-Atom Materials

Single-atom catalytic (SAC) materials refer to catalysts formed by highly dispersed isolated metal atoms on the surface of a support (such as carbon-based materials, metal oxides).[180] Their core features include atomic-level dispersion (close to 100% atomic utilization), uniform coordination environment (such as M-N_4, M-O_4), and strong metal support interactions. Compared to traditional nanoparticle catalysts, SACs significantly enhance catalytic activity and selectivity by precisely regulating the electronic structure of active sites.[181] Since the electronic magnetic moment of a single atom is jointly controlled by the coordination number, coordination atom type, symmetry, and carrier properties of the coordination environment, precise adjustment of the magnetic moment can be achieved by designing coordination structures, thereby optimizing its performance in magnetic field-enhanced catalysis.[182] For example, regulating the N coordination number of Fe SACs can balance the spin state and reaction activity, providing a theoretical basis for the design of magnetic water electrolysis catalysts.

Single-atom catalysts exhibit high catalytic performance due to high atom utilization, but are usually not magnetic at room temperature. Current research on single-atom catalysts focuses on increasing the loading of single atoms and enhancing the synergistic effect between atoms.[183,184] Coupling single-atom catalysts by an applied magnetic field can significantly improve their catalytic performance. Gd single-atom catalysts fixed on MoS_2 vacancies can be synthesized through laser molecular beam epitaxy. Due to the strong orbital hybridization between Gd-Mo-S atoms, Gd exhibits a magnetic moment of 0.829 μB. The alternating magnetic field can induce the spin direction of Gd to be flipped with the direction of the magnetic field, and localized heating is achieved at the active site. The localized heating of the active sites was achieved, the HER overpotential was reduced by 103 mV and the magnetothermal current was increased by nearly 924% under the effect of an alternating magnetic field of 3.9 mT (**Figure 17**a).[185] Gong et al. synthesized Co single-atom catalysts anchored in MoS_2 by laser molecular beam epitaxy, and the catalysts exhibited room-temperature ferromagnetism, and the OER overpotential was reduced by 67 mV at a current density of 10 mA cm^{-2} in an alternating magnetic field of 4.55 mT (Figure 17b).[186]

4.6. High-Entropy Alloys and Compounds

High-entropy alloys (HEAs) and compounds (HECs), composed of five or more principal elements in nearly equimolar ratios, form stable single-phase structures through entropy-driven suppression of phase separation.[187] Their compositional diversity,

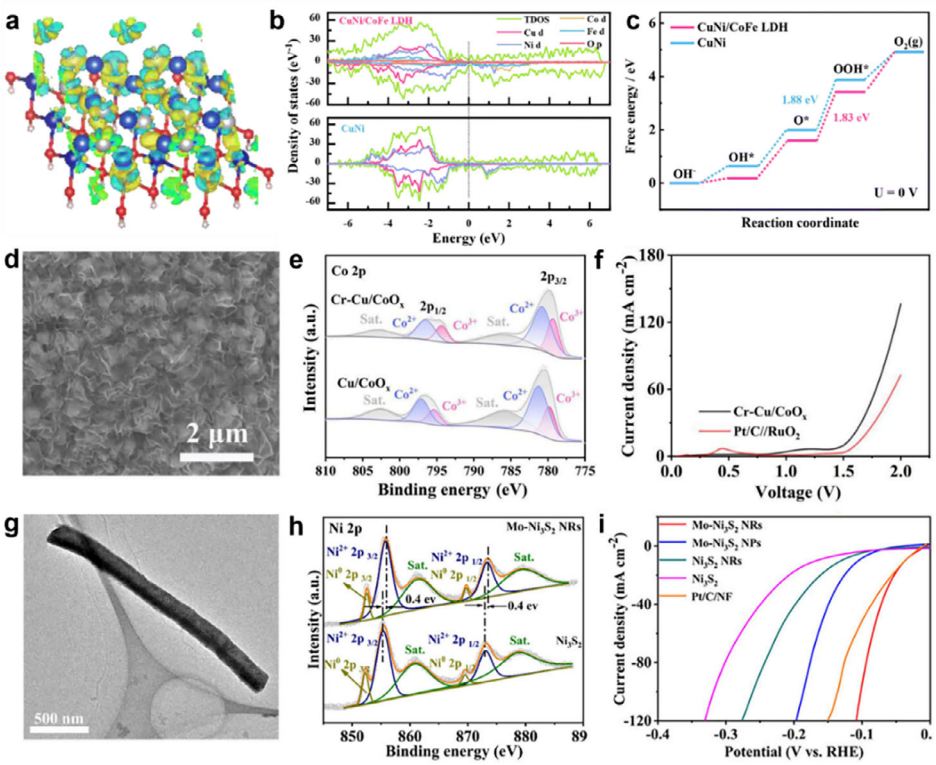

Figure 16. a) The charge density distribution of CuNi/CoFe LDH. b) The DOS of CuNi/CoFe LDH and CuNi. c) The free energy diagram for the OER on CuNi/CoFe LDH and CuNi; Adapted with permission.[179] Copyright 2024, Royal Society of Chemistry. d–f) Cr-Cu/CoOx nanosheet arrays morphology, electronic structure, and electrolytic water performance; Adapted with permission.[26] Copyright 2023, American Chemical Society. g–i) Mo-Ni_3S_2 nanorods morphology, electronic structure, and HER catalytic performance. Adapted with permission.[18] Copyright 2022, American Chemical Society.

lattice distortion, and sluggish diffusion kinetics endow them with exceptional mechanical strength, corrosion resistance, and catalytic activity.[188] In the context of water electrolysis, the synergistic effects of multiple metals (e.g., Co/Ni/Fe-based oxides) reduce reaction energy barriers by optimizing the adsorption energy of intermediates, while lattice distortion-induced electron redistribution and intrinsic corrosion resistance further enhance catalytic stability.[189]

The soft magnetic properties of HEAs, arising from multi-principal component synergy—such as high saturation magnetization, low coercivity, and high resistivity—effectively mitigate eddy current losses and enhance magnetic responsiveness. For instance, the $Al_{1.5}Co_4Fe_2Cr$ high-entropy alloy maintains high magnetic stability at elevated temperatures due to its coherent precipitation structure of BCC nanomagnetic particles within a B2 matrix, providing a robust foundation for efficient charge transfer under magnetic field modulation.[190] Moreover, the incorporation of magnetic elements (e.g., Fe, Co) in HEAs not only optimizes spin polarization properties but also fine-tunes the local electronic structure through short-range ordering (SRO) phenomena. This improves the efficiency of electron orbital hybridization and promotes the formation of spin-polarized current under magnetic field.[191] This accelerates the formation of O—O bonds in the OER process and promotes the reduction of H in HER. These unique magnetic properties, combined with the inherent structural and catalytic advantages of HEAs, position them as promising candidates for magnetic field-enhanced water electrolysis, offering pathways to improved efficiency and stability in green hydrogen production.

HEOs can optimize their magnetic and catalytic activity by controlling different heat treatment processes. Gao et al. synthesized $(FeCoNiCrMn)_3O_4$ spinel-structured HEO through electrospinning combined with quenching technology and explored the regulatory mechanism of quenching conditions (liquid nitrogen, ice water mixture, etc.) on its magnetic and catalytic properties.[192] The quenching process suppresses element segregation through rapid cooling, forms a single-phase cubic spinel structure, and significantly improves the saturation magnetization strength (the Ms of HEO-LN quenched in liquid nitrogen reaches 13.0 emug^{-1}, which is 78% higher than that of the naturally cooled sample). Its high magnetic responsiveness is due to the coherent precipitation and magnetic domain rearrangement of BCC nano magnetic particles and B2 matrix. After introducing an external magnetic field of 130 mT, HEO-LN was used as a spin polarizer to enhance electron spin polarization and reduce the energy barrier for O—O bond formation through quantum spin exchange interaction (QSEI). The OER overpotential decreased by 39.4 mV at 10 mA cm^{-1}, and the Tafel slope decreased from 80.43 to 71.38 mV dec^{-1}. This study provides new ideas for the design of magnetic high entropy materials and the magnetic field spin synergistic catalytic mechanism, promoting the development of efficient and low-energy green hydrogen preparation technology.

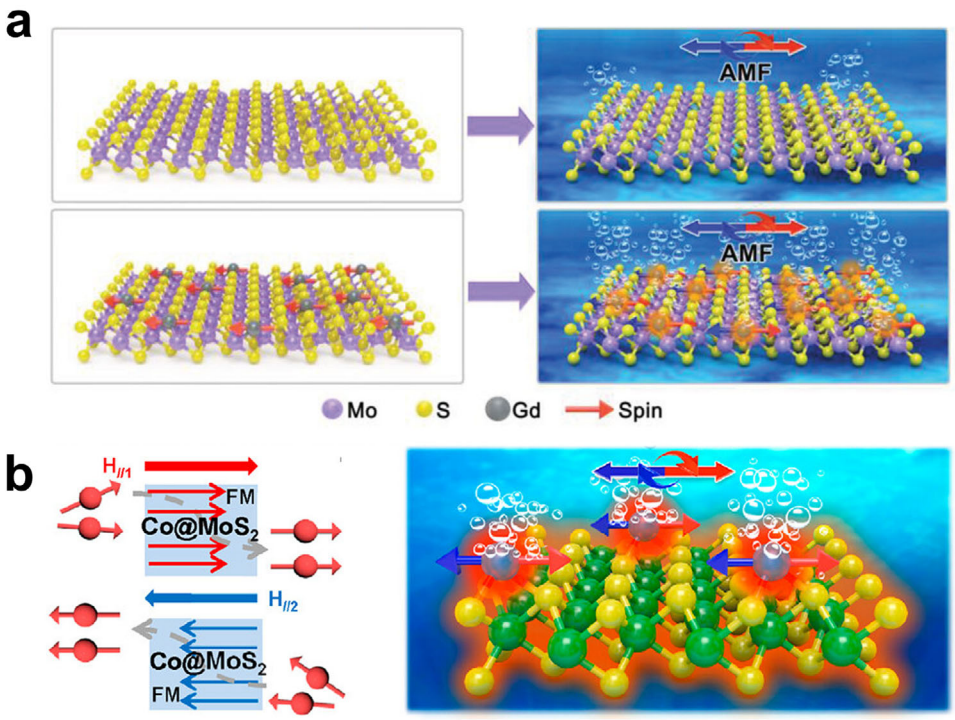

Figure 17. a) Schematic illustrating the AMF-assisted electrochemical HER process for $Sv@MoS_2$ and $Gd@MoS_2$; Adapted with permission.[185] Copyright 2022, John Wiley and Sons. b) Schematic diagram of the AMF-boosted $Co@MoS_2$ OER process by exploiting the magnetic heating generated from the spin polarization flip of the ferromagnetic SACs. Adapted with permission.[186] Copyright 2022, American Chemical Society.

4.7. Self-Supported Materials

Powdered catalysts are the most frequently reported type of catalysts; however, they require the addition of polymer binders (such as Nafion, polytetrafluoroethylene, etc.) to be loaded onto electrode substrates. This can lead to the coverage of some catalytic active sites and a reduction in electronic conductivity. To significantly increase the electrode's conductivity, conductive materials like carbon-based nanomaterials are typically added. However, carbon materials are susceptible to corrosion during electrochemical reactions, which can decrease the performance and stability of the electrode.[193] Self-supported electrodes exhibit a high specific surface area, exposing a greater number of active sites and stronger intrinsic activity. The strong binding between the catalyst and the substrate in self-supported electrodes can mitigate the detachment of the catalyst during the catalytic process.

Mu et al.[26] successfully fabricated self-supported Cr-Cu/CoO_x nanosheet arrays using electro-deposition and thermal annealing methods. The introduction of Cr promotes the generation of higher-valence Cu and Co, enhancing the d-band center of active sites and facilitating the dissociation of water molecules and the transformation of oxygen-containing intermediates. This results in overall water splitting performance superior to the Pt/C//RuO_2 system (Figure 16d–f). Wang et al.[18] introduced Mo into Ni_3S_2 through a hydrothermal method, promoting electron transfer from Ni to S, allowing Ni to act as a water dissociation and adsorption site, while S can serve as a hydrogen adsorption and desorption site. By adjusting the catalyst with NH4OH to form a nanorod structure, high-index crystal facets of the catalyst are exposed; the unique S atom coordination environment on these high-index facets more readily adsorbs intermediates, enhancing catalytic performance. Selecting ferromagnetic substrate materials and constructing self-supported electrodes that utilize spin polarization and spin pinning effects hold promise for achieving efficient and stable magnetic field-enhanced electrolytic water splitting (Figure 16g–i).

Traditional co-deposition methods face challenges in precisely controlling elemental ratios, primarily due to the preferential precipitation of certain elements that inhibit subsequent element deposition.[194] To address this issue, magnetic fields, as a non-invasive control method, offer new insights for optimizing catalyst composition through magnetohydrodynamic (MHD) effects and local microenvironment regulation. Hao et al.[195] successfully achieved precise control of the Ni/Fe ratio using magnetic field-assisted electrodeposition, constructing a self-supporting Ni-FeOOH/$Ni(OH)_2$ catalyst. Experimental results demonstrated that, compared to the non-magnetic field deposition system, the magnetic field significantly enhanced the deposition rate of Ni and suppressed the formation of heterostructures during FeOOH crystallization through microenvironment regulation and electronic structure optimization. This strategy reduced the overpotential of the catalyst by 34 mV at a current density of 20 mA cm^{-2}, providing an innovative solution for optimizing catalyst composition and enhancing performance.

The aforementioned various types of materials possess varying degrees of potential in the structure and performance of magnetic field-enhanced electrolytic water catalysts, providing broader ideas for the selection and design of future magnetic

Table 1. Overview of current magnetic field-enhanced electrochemical water splitting catalysts.

Catalyst	Pristine overpotential	Magnetic field effects	Enhancement	Electrolyte	Refs.
NiFe/NiFeOOH	η_{10} = 342 mV (OER)	MT	$\Delta\eta_{10}$ = 133 mV	1 M KOH	[82]
$Co_{0.8}Mn_{0.2}$-MOF	η_{100} = 310 mV (OER)	MT	$\Delta\eta_{100}$ = 120 mV	1 M KOH	[83]
a-NiFe@Ni-CW	η_{100} = 312 mV (OER)	MT	$\Delta\eta_{100}$ = 44 mV	1 M KOH	[84]
$NiSe_{2-x}$	η_{10} = 151 mV (HER)	MT	$\Delta\eta_{10}$ = 40 mV	1 M KOH	[81]
NiCoFe-MOF	η_{10} = 273 mV (OER)	MHD	$\Delta\eta_{10}$ = 59 mV	1 M KOH	[87]
Co_3O_4	η_{10} = 308 mV (OER)	MHD	$\Delta\eta_{10}$ = 56 mV	1 M KOH	[88]
NiFe LDH	η_{10} = 251 mV (OER)	MHD	$\Delta\eta_{10}$ = 42 mV	1 M KOH	[91]
$ZnCo_2O_4$	η_{10} = 406 mV (OER)	MHD	$\Delta\eta_{10}$ = 117 mV	1 M KOH	[92]
$NiFe_2O_4$@(Ni, Fe)P	η_{10} = 323 mV (OER)	MHD	$\Delta\eta_{10}$ = 147 mV	1 M KOH	[93]
$CoFe_2O_4$@CoBD	η_{10} = 341 mV (OER)	F_K	$\Delta\eta_{10}$ = 28 mV	1 M KOH	[99]
$Fe_{29}Co_{29}Ni_{29}P_{3.9}B_{9.1}$	η_{10} = 385 mV (HER)	F_L	$\Delta\eta_{10}$ = 35 mV	1 M KOH	[75]
Ni	η_{10} = 388 mV (OER)	MR	$\Delta\eta_{10}$ = 20 mV	1 M KOH	[29]
NCF–Co_3O_4	η_{10} = 547 mV (HER)	MR	$\Delta\eta_{10}$ = 70 mV	1 M KOH	[112]
MoS_2	η_{10} = 132 mV (HER)	SS	$\Delta\eta_{10}$ = 19 mV	1 M KOH	[116]
$Co_xNi_{1-x}Fe_2O_4$	η_{10} = 222 mV (OER)	SS	$\Delta\eta_{10}$ = 21 mV	1 M KOH	[120]
$CoFe_2O_4$	η_{10} = 418 mV (OER)	SS	$\Delta\eta_{10}$ = 68 mV	1 M KOH	[123]
Fe_3O_4@CNTs	η_{10} = 89 mV (HER) η_{100} = 243 mV (OER)	SS	$\Delta\eta_{10}$ = 67 mV (HER) $\Delta\eta_{100}$ = 64 mV (OER)	1 M KOH	[127]
Cu_1–Ni_6Fe_2–LDH	η_{10} = 210 mV (OER)	SS	$\Delta\eta_{10}$ = 30 mV	1 M KOH	[129]
$CoFe_2O_4$	η_{100} = 440 mV (OER)	SS	$\Delta\eta_{10}$ = 10 mV	1 M KOH	[130]
$CoFe_2O_4$/Co(Fe)O_xH_y	η_{10} = 300 mV (OER)	SP	$\Delta\eta_{10}$ = 10 mV	1 M KOH	[138]
LDH/Co_3O_4/NF	η_{50} = 274 mV (OER)	MR	$\Delta\eta_{50}$ = 25 mV	1 M KOH	[141]
Gd@MoS_2	η_{10} = 160 mV (HER)	MT	$\Delta\eta_{10}$ = 103 mV	1 M KOH	[185]
$(FeCoNiCrMn)_3O_4$	η_{10} = 359.7 mV (OER)	SS	$\Delta\eta_{10}$ = 39.4 mV	1 M KOH	[192]

field-enhanced catalysts. However, they are not entirely independent; appropriate material design strategies can prepare composite structure catalysts. These could help us achieve the design of efficient, low-cost magnetic catalysts and may further reveal the mechanisms by which magnetic fields affect electrolytic water splitting.

The summary of recent magnetic field-enhanced electrolytic water catalysts is shown in **Table 1**, where MT refers to magnetothermal, MHD is magnetohydrodynamics, MR refers to magnetoresistive, FK refers to Kelvin force, FL refers to Lorentz force, SS refers to spin selectivity, and SP refers to spin pinning.

5. Summary and Prospects

Magnetic field-coupled water electrolysis technology holds potential in enhancing reaction kinetics, optimizing catalyst performance, and improving device efficiency. However, several challenges remain to be addressed, such as the dissociation of magnetic field effects, the design of magnetic field devices, and the relationship between magnetic field strength and catalytic effects. To achieve widespread application, it is essential to conduct in-depth research into the specific mechanisms of magnetic field effects, develop adaptable and cost-effective magnetic materials, and optimize device structures. These efforts will provide more effective technical support for the transition to sustainable energy.

Firstly, the mechanisms through which magnetic fields influence reactions are not fully understood. While studies have explored the magneto-thermal effect, magnetohydrodynamic effect, and spin-polarization effect, other potential influencing mechanisms, such as the Kelvin force effect and Maxwell stress effect, require further research to fully exploit magnetic field-enhanced catalysis. Additionally, the research on how magnetic fields affect catalytic processes like HER and OER has not adequately differentiated between various catalytic mechanisms. The intrinsic relationship between catalytic mechanisms and catalyst magnetism remains unclear. For instance, in OER, various reaction mechanisms involve different active sites and intermediates that the magnetic field may influence differently. Identifying the actual active sites and understanding the catalytic mechanisms in magnetically-assisted processes are vital for designing highly sensitive magnetically responsive catalytic materials.

Moreover, the effect of magnetic fields on small molecule-coupled water electrolysis is not well-documented. Studying the influence of magnetic fields on alternative anodic oxidation processes, such as the Urea oxidation reaction, the methanol oxidation reaction, and the hydrazine oxidation reaction, could lead to more efficient and low-energy hydrogen production.

In terms of device implementation, while magnetic fields can enhance mass transfer at the catalyst-electrolyte interface and reduce ionic conduction resistance, their impact at higher current densities remains uncertain. Additionally, excessive magnetic fields might negatively affect other components of the electrolysis device, such as wires and control circuits. The challenge lies in designing magnetic field strengths and distributions that optimize device performance without increasing complexity and

cost. This requires a balanced approach to developing magnetically regulated water electrolysis systems, potentially integrated with other energy sources like solar and wind to enhance efficiency and stability.

Acknowledgements

The authors acknowledged financial support from the National Natural Science Foundation of China (U24A2039, 52222105), Zhejiang Provincial Natural Science Foundation of China (LR22E010004). G. Li thanks the support from Ningbo Yongjiang Talent Introduction Programme (2022A-090-G), the International Cooperation Project of Ningbo City (2024H007), and the Max Planck Partner Group program.

Conflict of Interest

The authors declare no conflict of interest.

Author Contributions

All authors jointly wrote the manuscript.

Keywords

electrocatalysts, hydrogen evolution reaction (HER), magnetic field, oxygen evolution reaction (OER)

Received: July 18, 2025
Published online: October 3, 2025

[1] T. Guo, L. Li, Z. Wang, *Adv. Energy Mater.* **2022**, *12*, 2200827.
[2] Z. Y. Yu, Y. Duan, X. Y. Feng, X. Yu, M. R. Gao, S. H. Yu, *Adv. Mater.* **2021**, *33*, 2007100.
[3] Q. Yan, J. Feng, W. Shi, W. Niu, Z. Lu, K. Sun, X. Yang, L. Xue, Y. Liu, Y. Li, B. Zhang, *Adv. Sci. (Weinh)* **2024**, *11*, 2402356.
[4] R. Zhang, T. Zhai, H. Wang, S. Lu, *Adv. Energy Sustain. Res.* **2024**, *5*, 2400085.
[5] L. Guo, J. Chi, T. Cui, J. Zhu, Y. Xia, H. Guo, J. Lai, L. Wang, *Adv. Energy Mater.* **2024**, *14*, 2400975.
[6] Y. Xu, C. Wang, Y. Huang, J. Fu, *Nano Energy* **2021**, *80*, 105545.
[7] L. Quan, H. Jiang, G. Mei, Y. Sun, B. You, *Chem. Rev.* **2024**, *124*, 3694.
[8] Z. W. Seh, J. Kibsgaard, C. F. Dickens, I. Chorkendorff, J. K. Norskov, T. F. Jaramillo, *Science* **2017**, *355*, eaad4998.
[9] H. Yang, Y. Liu, S. Luo, Z. Zhao, X. Wang, Y. Luo, Z. Wang, J. Jin, J. Ma, *ACS Catal.* **2017**, *7*, 5557.
[10] Z. Li, Y. Zhang, Y. Feng, C. Q. Cheng, K. W. Qiu, C. K. Dong, H. Liu, X. W. Du, *Adv. Funct. Mater.* **2019**, *29*, 1903444.
[11] H. Xue, H. Zhang, S. Fricke, M. Lüther, Z. Yang, A. Meng, W. Bremser, Z. Li, *Sustain. Energ. Fuels* **2020**, *4*, 1723.
[12] Q. Kang, D. Lai, W. Tang, Q. Lu, F. Gao, *Chem. Sci.* **2021**, *12*, 3818.
[13] Z. Wu, T. Wang, J.-J. Zou, Y. Li, C. Zhang, *ACS Catal.* **2022**, *12*, 5911.
[14] J. Sun, M. Dou, Z. Zhang, J. Ji, F. Wang, *Electrochim. Acta* **2016**, *215*, 447.
[15] C. Wang, P. Zou, W. Xu, Y. Zhang, J. Huo, J.-Q. Wang, Y. Liu, C. Qin, *J. Alloys Compd.* **2024**, *995*, 174790.
[16] C. Yu, X.-w. Wang, W.-x. He, Z.-y. Zheng, X.-j. Dang, Y.-f. Zhang, *Surf. Interfaces* **2024**, *46*, 104084.
[17] B. Chen, P. Hu, F. Yang, X. Hua, F. F. Yang, F. Zhu, R. Sun, K. Hao, K. Wang, Z. Yin, *Small* **2023**, *19*, 2207177.
[18] K. Wang, L. Yan, X. Mu, B. Feng, K. Lv, X. Yu, L. Li, X. Zhang, X. Yang, Z. Lu, *ACS A.E.M* **2022**, *5*, 11498.
[19] J. Liu, H. Yuan, Z. Wang, J. Li, M. Yang, L. Cao, G. Liu, D. Qian, Z. Lu, *Chem. Commun.* **2019**, *55*, 10860.
[20] S. Ju, J. Feng, P. Zou, W. Xu, S. Wang, W. Gao, H.-J. Qiu, J. Huo, J.-Q. Wang, *J. Mater. Chem. A* **2020**, *8*, 3246.
[21] L. Yang, R. He, M. Botifoll, Y. Zhang, Y. Ding, C. Di, C. He, Y. Xu, L. Balcells, J. Arbiol, Y. Zhou, A. Cabot, *Adv. Mater.* **2024**, 2400572.
[22] Y. Yan, J. Lin, K. Huang, X. Zheng, L. Qiao, S. Liu, J. Cao, S. C. Jun, Y. Yamauchi, J. Qi, *J. Am. Chem. Soc.* **2023**, *145*, 24218.
[23] Q. Yue, C. Liu, Y. Wan, X. Wu, X. Zhang, P. Du, *J. Catal.* **2018**, *358*, 1.
[24] Y. Liu, H. T. D. Bui, A. R. Jadhav, T. Yang, S. Saqlain, Y. Luo, J. Yu, A. Kumar, H. Wang, L. Wang, V. Q. Bui, M. G. Kim, Y. D. Kim, H. Lee, *Adv. Funct. Mater.* **2021**, *31*, 2010718.
[25] Y. Rao, S. Chen, Q. Yue, Y. Kang, *ACS Catal.* **2021**, *11*, 8097.
[26] X. Mu, K. Wang, K. Lv, B. Feng, X. Yu, L. Li, X. Zhang, X. Yang, Z. Lu, *ACS Appl. Mater. Interfaces* **2023**, *15*, 16552.
[27] Z.-L. Wang, G.-Y. Huang, G.-R. Zhu, H.-C. Hu, C. Li, X.-H. Guan, H.-B. Zhu, *Appl. Catal. B-Environ. Energy* **2025**, *361*, 124585.
[28] J. Thakur, P. Phogat, *Fuel* **2025**, *392*, 134954.
[29] Y. Zhang, P. Guo, S. Li, J. Sun, W. Wang, B. Song, X. Yang, X. Wang, Z. Jiang, G. Wu, P. Xu, *J. Mater. Chem. A* **2022**, *10*, 1760.
[30] Y. Zhou, Y. Hu, X. Gong, Z. Wang, S. Zhang, M. Wang, *Electrochim. Acta* **2018**, *284*, 560.
[31] Y. Zhou, Y. Ma, X. Wang, G. Yang, Y. Ding, Y. Cui, J. Zhang, H. Ge, J. Sun, *Adv. Funct. Mater.* **2023**, *33*, 2304296.
[32] J. H. Lee, W. S. Jang, S. W. Han, H. K. Baik, *Langmuir* **2014**, *30*, 9866.
[33] Y. Tong, L. Song, Y. Gao, L. Fan, F. Li, Y. Yang, G. Mo, Y. Liu, X. Shui, Y. Zhang, M. Gao, J. Huo, J. Qiao, E. Pineda, J.-Q. Wang, *Nat. Commun.* **2023**, *14*, 8407.
[34] K. Wang, Q. Yang, H. Zhang, M. Zhang, H. Jiang, C. Zheng, J. Li, *J. Mater. Chem. A* **2023**, *11*, 7802.
[35] C. X. Zhao, J. N. Liu, B. Q. Li, D. Ren, X. Chen, J. Yu, Q. Zhang, *Adv. Funct. Mater.* **2020**, *30*, 2003619.
[36] J. Yao, W. Huang, W. Fang, M. Kuang, N. Jia, H. Ren, D. Liu, C. Lv, C. Liu, J. Xu, Q. Yan, *Small Methods* **2020**, *4*, 2000494.
[37] H. Liu, Y. Ren, K. Wang, X. Mu, S. Song, J. Guo, X. Yang, Z. Lu, *Metals* **2022**, *12*, 800.
[38] F. Foroughi, C. Immanuel Bernäcker, L. Röntzsch, B. G. Pollet, *Ultrason. Sonochem.* **2022**, *84*, 105979.
[39] H. Wang, K. Wang, Y. Zuo, M. Wei, P. Pei, P. Zhang, Z. Chen, N. Shang, *Adv. Funct. Mater.* **2022**, *33*, 2210127.
[40] C. Biz, J. Gracia, M. Fianchini, *Int. J. Mol. Sci.* **2022**, *23*, 14768.
[41] C. Zhong, W. Zhou, X. Luo, T. Li, F. Huang, J. Hu, Z. Jiang, C. Hu, W. Lei, C. Yuan, *Nano Lett.* **2025**, *25*, 1550.
[42] Y. Sun, H. Lv, H. Yao, Y. Gao, C. Zhang, *Carbon Energy* **2024**, *6*, e575.
[43] G. Li, Q. Yang, K. Manna, Q. Mu, C. Fu, Y. Sun, C. Felser, *CCS Chemistry* **2021**, *3*, 2259.
[44] Y. Zhang, C. Liang, J. Wu, H. Liu, B. Zhang, Z. Jiang, S. Li, P. Xu, *ACS A.E.M* **2020**, *3*, 10303.
[45] J. O. Olowoyo, R. J. Kriek, *Small* **2022**, *18*, 2203125.
[46] H. Wu, Q. Huang, Y. Shi, J. Chang, S. Lu, *Nano Res.* **2023**, *16*, 9142.
[47] E. Skúlason, V. Tripkovic, M. E. Björketun, S. Gudmundsdóttir, G. Karlberg, J. Rossmeisl, T. Bligaard, H. Jo´nsson, J. K. Nørskov, *J. Phys. Chem. C* **2010**, *114*, 18182.
[48] L. Yang, Z. Liu, S. Zhu, L. Feng, W. Xing, *Mater. Today Phys* **2021**, *16*, 100292.
[49] C. Lin, J.-L. Li, X. Li, S. Yang, W. Luo, Y. Zhang, S.-H. Kim, D.-H. Kim, S. S. Shinde, Y.-F. Li, Z.-P. Liu, Z. Jiang, J.-H. Lee, *Nat. Catal.* **2021**, *4*, 1012.
[50] Y. Cheng, H. Wang, H. Song, K. Zhang, G. I. N. Waterhouse, J. Chang, Z. Tang, S. Lu, *Nano Research Energy* **2023**, *2*, 9120082.
[51] X. Ping, Y. Liu, L. Zheng, Y. Song, L. Guo, S. Chen, Z. Wei, *Nat. Commun.* **2024**, *15*, 2501.

[52] Y. Zhang, J. Kang, H. Xie, H. Yin, Z. Zhang, E. Liu, L. Ma, B. Chen, J. Sha, L. Qian, W. Hu, C. He, N. Zhao, *Appl. Catal. B-Environ.* **2024**, *341*, 123331.
[53] Q. Ji, B. Tang, X. Zhang, C. Wang, H. Tan, J. Zhao, R. Liu, M. Sun, H. Liu, C. Jiang, J. Zeng, X. Cai, W. Yan, *Nat. Commun.* **2024**, *15*, 8089.
[54] Y. Sun, S. Sun, H. Yang, S. Xi, J. Gracia, Z. J. Xu, *Adv. Mater.* **2020**, *32*, 2003297.
[55] H. Zhong, Q. Zhang, J. Yu, X. Zhang, C. Wu, H. An, Y. Ma, H. Wang, J. Zhang, Y.-W. Zhang, C. Diao, Z. G. Yu, S. Xi, X. Wang, J. Xue, *Nat. Commun.* **2023**, *14*, 7488.
[56] J. Roche, *Phys. Educ.* **1987**, *22*, 91.
[57] H. Griffiths, *IEEE Aerosp. Electron. Syst. Mag.* **2024**, *39*, 50.
[58] A. Rex, *Entropy* **2017**, *19*, 240.
[59] J. Romero Gómez, R. Ferreiro Garcia, A. De Miguel Catoira, M. Romero Gómez, *Renew. Sust. Energ. Rev.* **2013**, *17*, 74.
[60] G. E. Uhlenbeck, S. Goudsmit, *Nature* **1926**, *117*, 264.
[61] B. Iftikhar, M. Arshad Siddiqui, T. Javed, *Alex. Eng. J.* **2023**, *66*, 523.
[62] D. Liu, Y. Huang, J. Hu, B. Wang, Y. Lu, *ChemCatChem* **2022**, *14*, 202200889.
[63] J. B. Chen, J. Ying, Y. Tian, Y. X. Xiao, X. Y. Yang, *Adv. Funct. Mater.* **2024**, *35*, 2415660.
[64] S. J. Carey, W. Zhao, C. T. Campbell, *Angew. Chem.-Int. Edit.* **2018**, *57*, 16877.
[65] Z.-J. Zhang, N. Yu, Y.-L. Dong, G. Han, H. Hu, Y.-M. Chai, B. Dong, *Chem. Eng. J.* **2024**, *498*, 155736.
[66] S. Yang, X. Liu, S. Li, W. Yuan, L. Yang, T. Wang, H. Zheng, R. Cao, W. Zhang, *Chem. Soc. Rev.* **2024**, *53*, 5593.
[67] I. C. Man, H. Y. Su, F. Calle-Vallejo, H. A. Hansen, J. I. Martínez, N. G. Inoglu, J. Kitchin, T. F. Jaramillo, J. K. Nørskov, J. Rossmeisl, *ChemCatChem* **2011**, *3*, 1159.
[68] J. Suntivich, K. J. May, H. A. Gasteiger, J. B. Goodenough, Y. Shao-Horn, *Science* **2011**, *334*, 1383.
[69] Y. Duan, S. Sun, Y. Sun, S. Xi, X. Chi, Q. Zhang, X. Ren, J. Wang, S. J. H. Ong, Y. Du, L. Gu, A. Grimaud, Z. J. Xu, *Adv. Mater.* **2019**, *31*, 1807898.
[70] Z.-F. Huang, J. Song, Y. Du, S. Xi, S. Dou, J. M. V. Nsanzimana, C. Wang, Z. J. Xu, X. Wang, *Nat. Energy* **2019**, *4*, 329.
[71] G. Chen, Y. Sun, R. R. Chen, C. Biz, A. C. Fisher, M. P. Sherburne, J. W. Ager Iii, J. Gracia, Z. J. Xu, *J. Phys-Energy* **2021**, *3*, 031004.
[72] E. Torun, C. M. Fang, G. A. de Wijs, R. A. de Groot, *J. Phys. Chem. C* **2013**, *117*, 6353.
[73] Z. Luo, L. Zhang, L. Wu, L. Wang, Q. Zhang, X. Ren, X. Sun, *Nano Energy* **2022**, *102*, 107654.
[74] X. Ren, T. Wu, Y. Sun, Y. Li, G. Xian, X. Liu, C. Shen, J. Gracia, H.-J. Gao, H. Yang, Z. J. Xu, *Nat. Commun.* **2021**, *12*, 2608.
[75] L. Cai, J. Huo, P. Zou, G. Li, J. Liu, W. Xu, M. Gao, S. Zhang, J. Q. Wang, *ACS Appl. Mater. Interfaces* **2022**, *14*, 15243.
[76] J. A. Koza, S. Mühlenhoff, P. Żabiński, P. A. Nikrityuk, K. Eckert, M. Uhlemann, A. Gebert, T. Weier, L. Schultz, S. Odenbach, *Electrochim. Acta* **2011**, *56*, 2665.
[77] B. Seo, S. H. Joo, *Nat. Energy* **2018**, *3*, 451.
[78] B. Pierozynski, T. Mikolajczyk, *Electrocatalysis* **2014**, *6*, 51.
[79] C. Niether, S. Faure, A. Bordet, J. Deseure, M. Chatenet, J. Carrey, B. Chaudret, A. Rouet, *Nat. Energy* **2018**, *3*, 476.
[80] S. Ota, Y. Takemura, *J. Phys. Chem. C* **2019**, *123*, 28859.
[81] J. Huang, W. Zhou, X. Luo, Y. Ding, D. Peng, M. Chen, H. Zhou, C. Hu, C. Yuan, S. Wang, *Chem. Eng. J.* **2023**, *454*, 140279.
[82] D. Peng, C. Hu, X. Luo, J. Huang, Y. Ding, W. Zhou, H. Zhou, Y. Yang, T. Yu, W. Lei, C. Yuan, *Small* **2022**, *19*, 2205665.
[83] G. Zhou, P. Wang, H. Li, B. Hu, Y. Sun, R. Huang, L. Liu, *Nat. Commun.* **2021**, *12*, 4827.
[84] Y. Wang, X. Fan, Q. Du, Y. Shang, X. Li, Z. Cao, X. Wang, J. Li, Y. Xie, W. Gan, *Small* **2023**, *19*, 2206798.
[85] R. Aogaki, R. Morimoto, M. Asanuma, *J. Magn. Magn. Mater.* **2010**, *322*, 1664.
[86] V. Gatard, J. Deseure, M. Chatenet, *Curr. Opin. Electrochem.* **2020**, *23*, 96.
[87] H.-b. Zheng, Y.-l. Wang, P. Zhang, F. Ma, P.-z. Gao, W.-m. Guo, H. Qin, X.-p. Liu, H.-n. Xiao, *Chem. Eng. J.* **2021**, *426*, 130785.
[88] Y. Li, L. Zhang, J. Peng, W. Zhang, K. Peng, *J. Power Sources* **2019**, *433*, 226704.
[89] J. Sun, B. Yu, F. Tan, W. Yang, G. Cheng, Z. Zhang, *Int. J. Hydrogen Energy* **2022**, *47*, 15764.
[90] L. Elias, A. Chitharanjan Hegde, *Electrocatalysis* **2017**, *8*, 375.
[91] X. Qin, J. Teng, W. Guo, L. Wang, S. Xiao, Q. Xu, Y. Min, J. Fan, *Catal. Lett.* **2022**, *153*, 673.
[92] H.-b. Zheng, S.-q. Jing, Y.-l. Wang, P.-z. Gao, H. Qin, D.-y. Li, W.-m. Guo, X.-p. Liu, H.-n. Xiao, *Int. J. Hydrogen Energy* **2023**, *51*, 511.
[93] Y.-l. Wang, T.-h. Yang, S. Yue, H.-b. Zheng, X.-p. Liu, P.-z. Gao, H. Qin, H.-n. Xiao, *ACS Appl. Mater. Interfaces* **2023**, *15*, 11631.
[94] N. Bidin, S. R. Azni, S. Islam, M. Abdullah, M. F. S. Ahmad, G. Krishnan, A. R. Johari, M. A. A. Bakar, N. S. Sahidan, N. Musa, M. F. Salebi, N. Razali, M. M. Sanagi, *Int. J. Hydrogen Energy* **2017**, *42*, 16325.
[95] L. M. A. Monzon, J. M. D. Coey, *Electrochem. Commun.* **2014**, *42*, 42.
[96] A. A. Farmani, F. Nasirpouri, *J. Mater. Chem. A* **2020**, *8*, 24782.
[97] X. Li, C. Hao, Y. Du, Y. Lu, Y. Fan, M. Wang, N. Wang, R. Meng, X. Wang, Z. J. Xu, Z. Cheng, *Chin. J. Catal.* **2023**, *55*, 191.
[98] L. B. Wang, N I. Wakayama, T. Okada, *Electrochem. Commun.* **2002**, *4*, 584.
[99] S. Ma, K. Wang, M. Rafique, J. Han, Q. Fu, S. Jiang, X. Wang, T. Yao, P. Xu, B. Song, *Angew. Chem.-Int. Edit.* **2024**, *63*, 202412821.
[100] K. Stierstadt, M. Liu, *ZAMM – J. Appl. Math. Mech. /Zeitsch. Angewandte Mathem. Mech.* **2015**, *95*, 4.
[101] M. Mayur, S. Amiroudine, D. Lasseux, S. Chakraborty, *Electrophoresis* **2014**, *35*, 670.
[102] P. Connor, J. Schuch, B. Kaiser, W. Jaegermann, *Zeitschrift für Physikalische Chemie* **2020**, *234*, 979.
[103] O. Schnitzer, E. Yariv, *Phys Rev E Stat Nonlin Soft Matter Phys* **2013**, *87*, 041002.
[104] P. Dunne, J. M. D. Coey, *J. Phys. Chem. C* **2019**, *123*, 24181.
[105] A. A. Moya, *Phys. Chem. Chem. Phys.* **2015**, *17*, 5207.
[106] V. V. Prudnikov, P. V. Prudnikov, D. E. Romanovskiy, *J. Phys. D-Appl. Phys.* **2016**, *49*, 235002.
[107] X. H. Liu, C. F. Chang, L. H. Tjeng, A. C. Komarek, S. Wirth, *J. Phys. Condens. Matter.* **2019**, *31*, 225803.
[108] P. Corte-León, A. Gonzalez, V. Zhukova, M. Ipatov, J. M. Blanco, A. Zhukov, *J. Alloys Compd.* **2024**, *999*, 175023.
[109] S. Chatterjee, R. Maiti, D. Chakravorty, *RSC Adv.* **2020**, *10*, 13708.
[110] Y. Zhu, C.-Y. Huang, Y. Wang, D. Graf, H. Lin, S. H. Lee, J. Singleton, L. Min, J. C. Palmstrom, A. Bansil, B. Singh, Z. Mao, *Commun. Phys.* **2023**, *6*, 346.
[111] J. Li, Q. Pei, R. Wang, Y. Zhou, Z. Zhang, Q. Cao, D. Wang, W. Mi, Y. Du, *ACS Nano* **2018**, *12*, 3351.
[112] J. Saha, R. Ball, C. Subramaniam, *ACS Sustainable Chem. Eng.* **2021**, *9*, 7792.
[113] C. Biz, M. Fianchini, V. Polo, J. Gracia, *ACS Appl. Mater. Interfaces* **2020**, *12*, 50484.
[114] X. Li, Y. Bai, Z. Cheng, *Adv. Sci.* **2021**, *8*, 2101000.
[115] R. R. Chen, Y. Sun, S. J. H Ong, S. Xi, Y. Du, C. Liu, O. Lev, Z. J. Xu, *Adv. Mater.* **2020**, *32*, 1907976.
[116] W. Zhou, M. Chen, M. Guo, A. Hong, T. Yu, X. Luo, C. Yuan, W. Lei, S. Wang, *Nano Lett.* **2020**, *20*, 2923.
[117] J. Chen, Y. Ling, D. Qu, L. Huang, J. Li, P. Tang, A. He, X. Jin, Y. Zhou, M. Xu, J. Du, Z. Han, Q. Xu, *J. Alloys Compd.* **2021**, *877*, 160271.
[118] S. Xu, S. Feng, Y. Yu, D. Xue, M. Liu, C. Wang, K. Zhao, B. Xu, J. N. Zhang, *Nat. Commun.* **2024**, *15*, 1720.

[119] F. A. Garcés-Pineda, M. Blasco-Ahicart, D. Nieto-Castro, N. López, J. R. Galán-Mascarós, *Nat. Energy* **2019**, *4*, 519.
[120] Y. Ma, T. Wang, X. Sun, Y. Yao, H. Chen, G. Wu, C. Zhang, Y. Qin, *ACS Appl. Mater. Interfaces* **2023**, *15*, 7978.
[121] J. Qian, H. Zhang, G. Li, L. Jia, X. Peng, C. Zhong, F. Li, D. Chao, D. Gao, *Adv. Funct. Mater.* **2023**, *34*, 2305621.
[122] J. Ge, X. Ren, R. R. Chen, Y. Sun, T. Wu, S. J. H. Ong, Z. J. Xu, *Angew. Chem.-Int. Edit.* **2023**, *62*, 2301721.
[123] P. Guo, Y. Zhang, F. Han, Y. Du, B. Song, W. Wang, X. Wang, Y. Zhou, P. Xu, *J. Phys. Chem. Lett.* **2022**, *13*, 7476.
[124] W. Zhou, M. Chen, D. Zhao, C. Zhu, N. Wang, W. Lei, Y. Guo, L. Li, *Adv. Funct. Mater.* **2024**, *34*, 2402114.
[125] X. Ren, T. Wu, Z. Gong, L. Pan, J. Meng, H. Yang, F. B. Dagbjartsdottir, A. Fisher, H.-J. Gao, Z. J. Xu, *Nat. Commun.* **2023**, *14*, 2482.
[126] Q. Huang, S. Xie, J. Hao, Z. Ding, C. Zhang, H. Sheng, J. Zhao, *Angew. Chem.-Int. Edit.* **2023**, *62*, 2300469.
[127] H. Xue, J. Wang, H. Cheng, H. Zhang, X. Li, J. Sun, X. Wang, L. Lin, Y. Zhang, X. Liao, Y. He, *Appl. Catal. B-Environ. Energy* **2024**, *353*, 124087.
[128] J. Yan, Y. Wang, Y. Zhang, S. Xia, J. Yu, B. Ding, *Adv. Mater.* **2020**, *33*, 2007525.
[129] Z. Sun, L. Lin, J. He, D. Ding, T. Wang, J. Li, M. Li, Y. Liu, Y. Li, M. Yuan, B. Huang, H. Li, G. Sun, *J. Am. Chem. Soc.* **2022**, *144*, 8204.
[130] G. Song, M. Wei, J. Zhou, L. Mu, S. Song, *ACS Catal.* **2024**, *14*, 846.
[131] J. A. Carrasco, G. Abellán, E. Coronado, *J. Mater. Chem. C* **2018**, *6*, 1187.
[132] T. Sun, Z. Tang, W. Zang, Z. Li, J. Li, Z. Li, L. Cao, J. S. Dominic Rodriguez, C. O. M. Mariano, H. Xu, P. Lyu, X. Hai, H. Lin, X. Sheng, J. Shi, Y. Zheng, Y.-R. Lu, Q. He, J. Chen, K. S. Novoselov, C.-H. Chuang, S. Xi, X. Luo, J. Lu, *Nat. Nanotechnol.* **2023**, *18*, 763.
[133] L. Li, J. Zhou, X. Wang, J. Gracia, M. Valvidares, J. Ke, M. Fang, C. Shen, J. M. Chen, Y. C. Chang, C. W. Pao, S. Y. Hsu, J. F. Lee, A. Ruotolo, Y. Chin, Z. Hu, X. Huang, Q. Shao, *Adv. Mater.* **2023**, *35*, 2302966.
[134] L. Li, Y. Wang, R. R. Nazmutdinov, R. R. Zairov, Q. Shao, J. Lu, *Nano Lett.* **2024**, *24*, 6148.
[135] A. Zou, C. Wu, Q. Zhang, Y. Tang, J. Li, H. Meng, Z. Wang, C. Diao, Z. Yu, J. Xue, S. Xi, X. Wang, J. Wu, *Angew. Chem.-Int. Edit.* **2024**, *63*, 202409912.
[136] W. Zhang, H. Cao, X. Wen, L. Ma, Z. Zhang, Z. Xu, X. Luo, *Angew. Chem.-Int. Edit.* **2024**, *63*, 202411683.
[137] Z. Xiong, C. Hu, X. Luo, W. Zhou, Z. Jiang, Y. Yang, T. Yu, W. Lei, C. Yuan, *Nano Lett.* **2021**, *21*, 10486.
[138] T. Wu, X. Ren, Y. Sun, S. Sun, G. Xian, G. G. Scherer, A. C. Fisher, D. Mandler, J. W. Ager, A. Grimaud, J. Wang, C. Shen, H. Yang, J. Gracia, H.-J. Gao, Z. J. Xu, *Nat. Commun.* **2021**, *12*, 3634.
[139] J. Ge, R. R. Chen, X. Ren, J. Liu, S. J. H. Ong, Z. J. Xu, *Adv. Mater.* **2021**, *33*, 2101091.
[140] Y. Zhang, M. Chen, P. Guo, Y. Du, B. Song, X. Wang, Z. Jiang, P. Xu, *Carbon Energy* **2023**, *5*, e351.
[141] Y. Zhang, P. Guo, S. Niu, J. Wu, W. Wang, B. Song, X. Wang, Z. Jiang, P. Xu, *Small Methods* **2022**, *6*, 2200084.
[142] X. Lyu, Y. Zhang, Z. Du, H. Chen, S. Li, A. I. Rykov, C. Cheng, W. Zhang, L. Chang, W. Kai, J. Wang, L. Zhang, Q. Wang, C. Huang, E. Kan, *Small* **2022**, *18*, 2204143.
[143] L. H. Wong, M. G. Ahmed, Y. F. Tay, X. Chi, A. S. Razeen, Y. Fang, M. Zhang, A. Sng, S. Y. Chiam, A. Rusydi, *Angew. Chem.-Int. Edit.* **2024**, *64*, 202416757.
[144] W. H. Wang, *Prog. Mater. Sci.* **2019**, *106*, 100561.
[145] X. Liu, S. Ju, P. Zou, L. Song, W. Xu, J. Huo, J. Yi, G. Wang, J.-Q. Wang, *J. Alloys Compd.* **2021**, *880*, 160548.
[146] F. Han, Y. Chen, Y. Liu, X. Yang, S. Che, Y. Zhang, J. Huo, M. Gao, J.-Q. Wang, *Corros. Sci.* **2022**, *205*, 110420.
[147] J. Q. Wang, L. J. Song, J. T. Huo, M. Gao, Y. Zhang, *Adv. Mater.* **2024**, *36*, 2311406.
[148] Y. Q. Cheng, E. Ma, *Prog. Mater. Sci.* **2011**, *56*, 379.
[149] X. Li, W. Cai, D.-S. Li, J. Xu, H. Tao, B. Liu, *Nano Res.* **2021**, *16*, 4277.
[150] Y. Gao, Y. Tong, L. Song, J. Liu, B. Zang, M. Xiang, M. Gao, Y. Zhang, J. Huo, J.-Q. Wang, *EPJ Appl. Phys* **2023**, *98*, 20.
[151] H. X. Li, Z. C. Lu, S. L. Wang, Y. Wu, Z. P. Lu, *Prog. Mater. Sci.* **2019**, *103*, 235.
[152] F. Shen, B. Zang, L. Song, J. Huo, Y. Zhang, J.-Q. Wang, *Scr. Mater.* **2023**, *236*, 115666.
[153] S. Zhang, Y. Fan, Y. Li, W. Li, H. Yi, H. Li, T. Wang, J.-Q. Wang, F. Li, *Intermetallics* **2022**, *141*, 107395.
[154] L. Song, Y. Gao, P. Zou, W. Xu, M. Gao, Y. Zhang, J. Huo, F. Li, J. Qiao, L.-M. Wang, J.-Q. Wang, *Proc. Natl. Acad. Sci. USA* **2023**, *120*, 2302776120.
[155] L. J. Song, M. Gao, W. Xu, J. T. Huo, J. Q. Wang, R. W. Li, W. H. Wang, J. H. Perepezko, *Acta Mater.* **2020**, *185*, 38.
[156] M. Pan, H. Feng, Z. Zhang, M. Gao, L. Lei, D. Wang, G. Li, J. Huo, J.-Q. Wang, *J. Mater. Chem. A* **2024**, *12*, 15334.
[157] X. Liu, P. Zou, L. Song, B. Zang, B. Yao, W. Xu, F. Li, J. Schroers, J. Huo, J.-Q. Wang, *ACS Catal.* **2022**, *12*, 3789.
[158] X. Yu, X. Gong, H. Qiao, X. Liu, C. Ma, R. Xiao, R. Li, T. Zhang, *Small Methods* **2024**, *8*, 2400793.
[159] B. Li, S. D. Jiang, Q. Fu, R. Wang, W. Z. Xu, J. X. Chen, C. Liu, P. Xu, X. J. Wang, J. H. Li, H. B. Fan, J. T. Huo, J. F. Sun, Z. L. Ning, B. Song, *Adv. Funct. Mater.* **2024**, *35*, 2413088.
[160] H. Liu, X. H. Zhang, Y. X. Li, X. Li, C. K. Dong, D. Y. Wu, C. C. Tang, S. L. Chou, F. Fang, X. W. Du, *Adv. Energy Mater.* **2020**, *10*, 1902521.
[161] B. A. Bernevig, C. Felser, H. Beidenkopf, *Nature* **2022**, *603*, 41.
[162] B. Yan, C. Felser, *Annu. Rev. Condens. Matter Phys.* **2017**, *8*, 337.
[163] A. Lau, C. Ortix, *Phys. Rev. Lett.* **2019**, *122*, 186801.
[164] G. Li, C. Felser, *Appl. Phys. Lett.* **2020**, *116*, 070501.
[165] C. Fu, S. N. Guin, T. Scaffidi, Y. Sun, R. Saha, S. J. Watzman, A. K. Srivastava, G. Li, W. Schnelle, S. S. P. Parkin, C. Felser, J. Gooth, *Research* **2020**, *2020*, 4643507.
[166] G. Li, Q. Xu, W. Shi, C. Fu, L. Jiao, M. E. Kamminga, M. Yu, H. Tüysüz, N. Kumar, V. Süß, R. Saha, A. K. Srivastava, S. Wirth, G. Auffermann, J. Gooth, S. Parkin, Y. Sun, E. Liu, C. Felser, *Sci. Adv.* **2019**, *5*, aaw9867.
[167] G. Li, Y. Xu, Z. Song, Q. Yang, Y. Zhang, J. Liu, U. Gupta, V. Süβ, Y. Sun, P. Sessi, S. S. P. Parkin, B. A. Bernevig, C. Felser, *Adv. Mater.* **2022**, *34*, 2201328.
[168] G. Li, C. Fu, W. Shi, L. Jiao, J. Wu, Q. Yang, R. Saha, M. E. Kamminga, A. K. Srivastava, E. Liu, A. N. Yazdani, N. Kumar, J. Zhang, G. R. Blake, X. Liu, M. Fahlman, S. Wirth, G. Auffermann, J. Gooth, S. Parkin, V. Madhavan, X. Feng, Y. Sun, C. Felser, *Angew. Chem.-Int. Edit.* **2019**, *58*, 13107.
[169] H. Qin, Y. He, P. Xu, D. Huang, Z. Wang, H. Wang, Z. Wang, Y. Zhao, Q. Tian, C. Wang, *Adv. Colloid Interface Sci.* **2021**, *294*, 102486.
[170] R. R. Krishnan, A. T. Prasannakumar, S. R. Chandran, K. H. Prema, *J. Mater. Sci.-Mater. Med.* **2022**, *33*, 17100.
[171] Y. S. Vidya, H. C. Manjunatha, K. N. Sridhar, L. Seenappa, R. Munirathnam, B. Chinnappareddy, *Inorg. Chem. Commun.* **2023**, *158*, 111408.
[172] M. Hassan, Y. Slimani, M. A. Gondal, M. J. S. Mohamed, S. Güner, M. A. Almessiere, A. M. Surrati, A. Baykal, S. Trukhanov, A. Trukhanov, *Ceram. Int.* **2022**, *48*, 24866.
[173] B. Debnath, S. Parvin, H. Dixit, S. Bhattacharyya, *ChemSusChem* **2020**, *13*, 3875.
[174] X. Zhang, L. Li, K. Cheng, Y. Wang, *Carbon* **2024**, *216*, 118513.
[175] T. Xia, Q. Ren, J. Yang, Z. Li, M. Shao, X. Duan, *Chem. Res. Chin. Univ.* **2024**, *40*, 577.
[176] L. Li, S. Lu, Y. Dai, H. Li, X. Wang, Y. Zhang, *ACS Appl. Nano Mater* **2023**, *6*, 2184.

[177] Y. Ye, H. Li, J. Cao, X. Liu, H. Fan, M. Wei, L. Yang, J. Yang, Y. Chen, *Int. J. Hydrogen Energy* **2023**, *48*, 17026.
[178] S.-L. Zheng, H.-M. Xu, H.-R. Zhu, T.-Y. Shuai, Q.-N. Zhan, C.-J. Huang, G.-R. Li, *J. Mater. Chem. A* **2024**, *12*, 18832.
[179] D. Wang, Y. Chu, Y. Wu, M. Zhu, L. Pan, R. Li, Y. Chen, W. Wang, N. Mitsuzaki, Z. Chen, *J. Mater. Chem. A* **2024**, *12*, 33680.
[180] B. Qiao, A. Wang, X. Yang, L. F. Allard, Z. Jiang, Y. Cui, J. Liu, J. Li, T. Zhang, *Nat. Chem.* **2011**, *3*, 634.
[181] Y. Li, Y. Liu, M. Guo, M. Li, H. Hao, C. Wang, L. Jin, C. Zhao, X. Shao, X. Yu, *Adv. Funct. Mater.* **2025**, 2425056.
[182] J. Cui, X. Yu, X. Li, J. Yu, L. Peng, Z. Wei, *Chin. J. Catal.* **2025**, *69*, 17.
[183] P. Kumar, K. Kannimuthu, A. S. Zeraati, S. Roy, X. Wang, X. Wang, S. Samanta, K. A. Miller, M. Molina, D. Trivedi, J. Abed, M. A. Campos Mata, H. Al-Mahayni, J. Baltrusaitis, G. Shimizu, Y. A. Wu, A. Seifitokaldani, E. H. Sargent, P. M. Ajayan, J. Hu, M. G. Kibria, *J. Am. Chem. Soc.* **2023**, *145*, 8052.
[184] J. Chang, Y. Shi, H. Wu, J. Yu, W. Jing, S. Wang, G. I. N. Waterhouse, Z. Tang, S. Lu, *J. Am. Chem. Soc.* **2024**, *146*, 12958.
[185] W. Zeng, Z. Jiang, X. Gong, C. Hu, X. Luo, W. Lei, C. Yuan, *Small* **2023**, *19*, 2206155.
[186] X. Gong, Z. Jiang, W. Zeng, C. Hu, X. Luo, W. Lei, C. Yuan, *Nano Lett.* **2022**, *22*, 9411.
[187] K. Wang, Y. Wang, Y. Chen, G. Deng, Y. Zhou, C. Xu, *Int. J. Hydrogen Energy* **2025**, *109*, 1108.
[188] Y. Zhang, Y. Cai, Y. Ding, *Chem. Commun.* **2025**, *61*, 4279.
[189] Y. Zhou, X. Shen, M. Wang, L. Zhang, T. Qian, C. Yan, J. Lu, *Sci. China Mater.* **2023**, *66*, 2527.
[190] C. Yang, J. Zhang, M. Li, X. Liu, *Acta Metall. Sin. (Engl. Lett.)* **2020**, *33*, 1124.
[191] Z. Wang, J. You, Y. Zhao, R. Yao, G. Liu, J. Lu, S. Zhao, *J. Environ. Chem. Eng.* **2023**, *11*, 109080.
[192] Z. Gao, J.-H. Liu, S. Wang, W. Yang, W. Wang, L. Li, H. Guo, J. Zheng, S. Ramakrishna, J. Zhang, L. Yang, Y.-Z. Long, *Chem. Eng. J.* **2024**, *496*, 154216.
[193] H. Yang, M. Driess, P. W. Menezes, *Adv. Energy Mater.* **2021**, *11*, 2102074.
[194] D. Li, T. Shan, C. Liu, C. Zhao, A. Doherty, A. R. Kamali, Q. Wang, *New J. Chem.* **2023**, *47*, 13098.
[195] X. Hao, F. Chen, Y. Zhang, Y. Liu, G. Gao, Y. Song, M. Xu, C. Sun, X. Zhang, Z. Lu, H. Dong, F. Lu, W. Wang, H. Liu, H. Liu, R. Zheng, Y. Cheng, *Materials Today Sustainability* **2023**, *24*, 100556.

Ziyong Zhang is a M.S. student at the School of Materials Science and Engineering, Hebei University of Technology. He obtained his bachelor's degree from Hebei University of Technology in 2020. His current research interests focus on magnetic field enhanced amorphous catalyst for water electrolysis.

Bo Feng is a Ph.D. student at the School of Materials Science and Engineering, Hebei University of Technology. He obtained his bachelor*'s degree from Hebei University of Technology in 2021. His current research interests focus on magnetic field coupled electrocatalysis for energy conversion.

Junting Sun received her Ph.D. from the Beijing University of Chemical Technology. She is currently a professor at School of Materials and Environmental Engineering, Hangzhou University of Electronic Science and Technology. His research focuses on transition metal compounds, carbon functional nanomaterials, magnetic material interface design, and anti-corrosion research. She has published more than 20 papers in international journals.

Guowei Li received his Ph.D. from the University of Groningen and was a post-doctoral fellow and group leader at the Max Planck Institute for Chemical Physics of Solids. He is currently a professor at Ningbo Institute of Materials Technology and Engineering, Chinese Academy of Sciences, and serves as the deputy director of the Key Laboratory of Magnetic Materials and Devices, CAS. His research focuses on spin chemistry, chiral effects of topological/magnetic crystals, and energy catalysis.

Zunming Lu is a professor at the School of Materials Science and Engineering, Hebei University of Technology. He received his Ph.D. in Materials Physics and Chemistry from Hebei University of Technology in 2007 and worked as a visiting scholar at the Electron Microscopy and Microanalysis Research Center at the University of Sydney from 2014 to 2015. His research interests focus on the design of metal based electrocatalytic materials and the mechanism study of magnetic catalytic materials. He has published more than 50 papers in international journals.

Jun-Qiang Wang is a professor in Ningbo Institute of Materials Technology and Engineering, Chinese Academy of Science. He got PhD from Institute of Physics CAS in 2010, and worked as a postdoc in Tohoku University and University of Wisconsin-Madison from 2010 to 2014. His research interests cover the physical and chemical properties of amorphous materials including metallic glasses, lunar glasses, chalcogenide glasses, etc. He has published more than 100 papers in PNAS, Phys. Rev. Lett., Nature Commun., Adv. Mater., ACS Catal., etc. He was awarded the National Outstanding Youth Fund and Young Scientist Award from 19th ISMANAM. Group website: https://non-crystal.nimte.ac.cn/.

Juntao Huo is a professor in Ningbo Institute of Materials Technology and Engineering, Chinese Academy of Science. He received his Ph.D. in condensed-matter physics from Institute of Physics, Chinese Academy of Sciences in 2012. His research interests focus on the design of novel amorphous alloys and the study of their functional properties. He has published more than 100 papers in international journals.